DTU Library

The velocity field induced by a helical vortex tube

Fukumoto, Y.; Okulov, Valery

Link back to DTU Orbit

The velocity field induced by a helical vortex tube

Y. Fukumoto[a)]
*Graduate School of Mathematics and Space Environment Research Center, Kyushu University 33,
Fukuoka 812-8581, Japan*

V. L. Okulov[b)]
*Department of Mechanical Engineering, Technical University of Denmark,
DK-2800 Kongens Lyngby, Denmark*

The influence of finite-core thickness on the velocity field around a vortex tube is addressed. An asymptotic expansion of the Biot-Savart law is made to a higher order in a small parameter, the ratio of core radius to curvature radius, which consists of the velocity field due to lines of monopoles and dipoles arranged on the centerline of the tube. The former is associated with an infinitely thin core and is featured by the circulation alone. The distribution of vorticity in the core reflects on the strength of dipole. This result is applied to a helical vortex tube, and the induced velocity due to a helical filament of the dipoles is obtained in the form of the Kapteyn series, which augments Hardin's [Phys. Fluids **25**, 1949 (1982)] solution for the monopoles. Using a singularity-separation technique, a substantial part of the series is represented in a closed form for both the mono- and the dipoles. It is found from numerical calculation that the smaller the helix pitch is, the larger the relative influence of the dipoles is as the cylinder wound by the helix is approached. © *2005 American Institute of Physics.* [DOI: 10.1063/1.2061427]

I. INTRODUCTION

Concentrated helical vortices are ubiquitous structures in swirling flows. Among them are breakdown of vortex filaments generated over a delta wing at a high angle of attack, trailing vortices behind an aircraft, tip vortex cords connected with blades of a propeller, tornadoes emerging in a cyclone core, concentrated vortices in swirl flows in many technological vortex devices, etc.

For a century, knowledge of motion of a slender helical vortex filament and of induced velocity field around it has continuously been growing. Unlike circular vortex rings, the Biot-Savart law cannot be integrated in a closed form even for a helical filament of infinitesimal thickness. In the case of an unbounded fluid, a representation for the velocity field is available in the form of an infinite series of twisted products of the modified cylindrical functions, namely, Kapteyn's-type series, by Hardin.[1] A precise knowledge of the velocity field in the vicinity of the core is requisite for working out the self-induced motion of a helical vortex filament, and much effort has been made to numerically and asymptotically evaluate the Biot-Savart law.[2–5] A comparison among several methods for deriving the filament speed was performed by Ricca[6] with a particular emphasis put on the effect of torsion. An efficient technique for elaborating the principal parts of the Kapteyn series was developed by Kuibin and Okulov.[7] Boersma and Wood[8] manipulated an integral representation of the Kapteyn series and made a thorough analysis of it. The Kapteyn series gets along with a circular cylindrical boundary, coaxial to the axis of the supporting cylinder.[7,9] A flow

with helical symmetry is amenable to a detailed analysis of the Euler equations. A theorem on the existence of a slender helical vortex tube was given by Adebiyi.[10] However, at present, available explicit solutions are limited to a circular cylindrical core or the limiting case of infinite pitch.[11–13]

Vortices observed in nature and created in laboratory are not necessarily thin. Despite this long history, the method is far from developed of how to treat a helical vortex tube of finite thickness whose centerline may be, to a large extent, deviated from a straight line. One of the prevailing methods is the cut-off method and its refinement, for a slender vortex tube, in which the Biot-Savart integral is approximated by a line integral and the logarithmic infinity of the integral on the core itself is disingularized so as not to be in contradiction in the known cases of vortex rings and infinitesimal vibrations of the Rankine vortex.[4,5,7,14] This approximation fails to take account of the influence of finite thickness of the distant parts. This paper presents an efficient machinery to make feasible a systematic handling of the Biot-Savart law for vorticity distributions localized in a tube-like structure.

As a by-product born in the study of the Saturn ring, Dyson[15] contrived an ingenious technique for evaluating, with a high accuracy, the velocity field in the neighborhood of the core of an axisymmetric vortex ring with vorticity proportional to the distance from the symmetric axis. He took advantage of a shift operator and an identity of a harmonic function and carried through efficient asymptotic expansions of the velocity field near the core to a high order in a small parameter, the ratio of the core radius to the ring radius. He thereby achieved a higher-order extension of Kelvin's formula of vortex-ring speed.[15,16] Recently, this technique was adapted to an axisymmetric vortex ring of an arbitrary distribution of vorticity and the formula for speed

---

[a)]Electronic mail: yasuhide@math.kyushu-u.ac.jp
[b)]Permanent address: Institute of Thermophysics, Novosibirsk 630090, Russia. Electronic mail: vokulov@mail.ru

of a viscous vortex ring[17,18] was extended to a higher order.[19] In effect, Dyson's technique is indispensable for pursuing higher-order asymptotics since otherwise expansions would suffer from a flood of terms that are out of control.

In the present investigation, we shall make an attempt to lift the restriction of axisymmetry of Dyson's method, whereby the influence of finite-core area of a curved vortex tube is incorporated successively in the form of multipole expansions. The small parameter ϵ is the ratio of the core radius to the typical curvature radius. With the aid of shift operators, integration over the core cross section, in the volume integral, is implemented first, leaving line integrals. The leading-order term of the Biot-Savart law coincides with the traditional approximation by a line of *monopole singularities* arranged on the centerline of the vortex tube. The monopole strength is equal to the circulation carried by the tube. This is followed by the contribution from a line of *dipoles* whose strength depends on the vorticity distribution in the core. The source for the dipoles is attributable to the influence of the centerline curvature.[16,19] Intriguingly there is an approach of evaluating the Biot-Savart law that lies in the other extreme; Levi-Civita[20] first integrated along the centerline and then collected the line integrals over the core.[21]

The latter half of this paper highlights a helical vortex tube. As with the case of the monopoles, the velocity field and the streamfunction for the helical dipole filament take the form of Kapteyn's-type series. By invoking the singularity-separation technique,[22] an infinite summation of the dominant parts collapses, with a sufficient accuracy, to a closed form.

In Sec. II, we expound the asymptotic development of the Biot-Savart law for a three-dimensional vortex tube. A brief outline of the asymptotic expansions, along with a version of the localized induction approximation (LIA), was reported in a previous paper.[23] A proof was given to the well posedness of the filament equation in the higher-order LIA.[24] This procedure necessitates the distribution of vorticity to $O(\epsilon^2)$. It is supplied by solving the Euler equations near the core, and thus we are led to inner and outer expansions. The Euler equations expressed in the local moving cylindrical coordinates are accommodated in Appendix A. The inner solution is constructed in a closed form, to the desired order, in Appendix B. The result so far is applicable to a three-dimensional vortex tube in general. We then specialize the asymptotic expansions to a helical vortex tube. Hardin's solution and the procedure of separating its singular terms are extended in Sec. III to encompass the higher-order field. Here we handle the vector potential for the velocity field as a fundamental entity. The streamfunction for a helically symmetric flow is manufactured by a combination of the components of the vector potential. In Sec. IV, we proceed to the dipole integral. The numerical calculation of the dipole terms is performed, and the importance of the dipoles relative to the monopoles is discussed. Section V is devoted to a summary and conclusions.
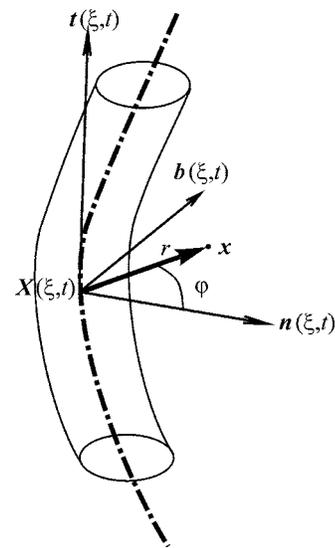

FIG. 1. Local coordinate system moving with a curved vortex tube.

II. ASYMPTOTIC DEVELOPMENT OF BIOT-SAVART LAW

We extend Dyson's technique[15,16,19] for the Biot-Savart law to three dimensions.[23] The formula obtained in this section is applicable to a general curved vortex tube with vorticity profile uniform along the tube.

A. Setting of coordinates

In order to represent a curved vortex tube, it is expedient to introduce local coordinates $(\tilde{x}, \tilde{y}, \xi)$, along with local cylindrical coordinates (r, φ, ξ) such that $\tilde{x} = r \cos \varphi$ and $\tilde{y} = r \sin \varphi$, moving with the filament (Fig. 1).[5,25,26] Here ξ is a parameter along the central curve X of the vortex tube, defined so as to satisfy $\dot{X}(\xi,t) \cdot t(\xi,t) = 0$. Here the Frenet-Serret frame (t, n, b), with t being the unit tangent vector, is employed, and a dot stands for a derivative in t with fixing ξ. Given a point $\mathbf{x}$ sufficiently close to the core, there corresponds uniquely the nearest point $X(\xi,t)$ on the centerline of the filament. Then $\mathbf{x}$ is expressed as

$$\mathbf{x} = X(\xi,t) + r \cos \varphi n(\xi,t) + r \sin \varphi b(\xi,t). \tag{1}$$

The coordinates (r, φ, ξ) are converted into orthogonal ones (r, θ, ξ) by *untwisting* the origin of angle by an integral of torsion $\tau(s,t)$ as

$$\theta(\varphi,\xi,t) = \varphi - \int_{s_0}^{s(\xi,t)} \tau(s',t) ds', \tag{2}$$

where $s = s(\xi,t)$ is the arclength parametrizing the centerline of the tube.

We define the velocity (u, v, w) as functions of r, θ, ξ and t, relative to the moving frame, by

$$u = \dot{X}(\xi,t) + u e_r + v e_\theta + w t, \tag{3}$$

where e_r and e_θ are the unit vectors in the radial and azimuthal directions, respectively. The components of the vorticity vector $\omega = \nabla \times u = \omega_r e_r + \omega_\theta e_\theta + \zeta t$ are calculable through

$$\omega_r = \frac{1}{r}\frac{\partial w}{\partial \theta} - \frac{1}{h_3}\frac{\partial v}{\partial \xi} + \frac{\eta}{h_3}\kappa w \sin\varphi - \frac{1}{h_3}\frac{\partial \dot{X}}{\partial \xi}\cdot \boldsymbol{e}_\theta,$$ (4)

$$\omega_\theta = -\frac{\partial w}{\partial r} + \frac{1}{h_3}\frac{\partial u}{\partial \xi} + \frac{\eta}{h_3}\kappa w \cos\varphi + \frac{1}{h_3}\frac{\partial \dot{X}}{\partial \xi}\cdot \boldsymbol{e}_r,$$ (5)

$$\zeta = \frac{1}{r}\frac{\partial}{\partial r}(rv) - \frac{1}{r}\frac{\partial u}{\partial \theta},$$ (6)

where $\kappa = \kappa(s,t)$ is the curvature of the centerline and

$$\eta = |\partial X/\partial \xi|, \quad h_3 = \eta(1 - \kappa r \cos\varphi).$$ (7)

B. Contribution from longitudinal vorticity

We confine ourselves to a *quasisteady* motion of a vortex filament. Suppose that the vorticity is dominated by the tangential component ζ. Allowance is made for a weak dependence on t. We stipulate that $|\zeta|$ decays sufficiently rapidly to zero with distance $r = (\tilde{x}^2 + \tilde{y}^2)^{1/2}$ from the vortex centerline so that all of its moment converges,

$$\int\int |\zeta(\tilde{x},\tilde{y})| r^n d\tilde{x} d\tilde{y} < \infty \quad (n = 0,1,2,\cdots).$$ (8)

We exclusively handle the vector potential $A(\mathbf{x})$ rather than the velocity $\mathbf{u} = \nabla \times A$. Imposition of the Coulomb-gauge condition

$$\nabla \cdot A = 0,$$ (9)

yields

$$A(\mathbf{x}) = \frac{1}{4\pi}\int\int\int \frac{\boldsymbol{\omega}(\mathbf{x}')}{|\mathbf{x} - \mathbf{x}'|}dV'.$$ (10)

In this integral, the contribution $A_\parallel$ from the longitudinal vorticity ζt is

$$A_\parallel(\mathbf{x}) = \frac{1}{4\pi}\int\int\int \frac{\zeta(\tilde{x},\tilde{y},s)t(s)(1-\kappa\tilde{x})}{|\mathbf{x} - X - \tilde{x}\mathbf{n} - \tilde{y}\boldsymbol{b}|}d\tilde{x}d\tilde{y}ds.$$ (11)

The factor $1 - \kappa\tilde{x}$ comes from the determinant of the Jacobian matrix $\partial(x,y,z)/\partial(\tilde{x},\tilde{y},s)$ between the global Cartesian coordinates (x,y,z) and the local ones $(\tilde{x},\tilde{y},s)$. Our assumption of the slenderness of the tube guarantees that $1 - \kappa\tilde{x} > 0$ in the core which shares almost all contribution to the integral.

With the aid of shift operators, (11) is formally cast into

$$A_\parallel(\mathbf{x}) = \frac{1}{4\pi}\int ds\left\{\int\int d\tilde{x}d\tilde{y}\zeta(\tilde{x},\tilde{y},s)(1 - \kappa\tilde{x})\right.$$
$$\left. \times \exp[-\tilde{x}(\mathbf{n}\cdot\nabla) - \tilde{y}(\boldsymbol{b}\cdot\nabla)]\right\}\frac{t(s)}{|\mathbf{x} - X(s)|}.$$ (12)

The exponential function endowed with the operator ∇ acts to replace $\mathbf{x}$ with $\mathbf{x} - \tilde{x}\mathbf{n} - \tilde{y}\boldsymbol{b}$ in the function that follows. This is an extension, to three dimensions, of Dyson's technique[15] which was originally devised for an axisymmetric vortex ring.

A broaden vorticity distribution is incorporated successively in the form of multipoles by expanding the exponential function in Taylor series with respect to its argument. In

this, ∇ should be taken to be unrelated to the variables $\tilde{x}$, $\tilde{y}$, and s. In order to gain a correction to the traditional formula, it is necessary to expand to the following order:

$$A_\parallel(\mathbf{x}) = \frac{1}{4\pi}\int ds\left\{\int\int d\tilde{x}d\tilde{y}\zeta(\tilde{x},\tilde{y},s)\left(1 - \kappa\tilde{x} - \tilde{x}(\mathbf{n}\cdot\nabla)\right.\right.$$
$$- \tilde{y}(\boldsymbol{b}\cdot\nabla) + \frac{1}{2}[\tilde{x}^2(\mathbf{n}\cdot\nabla)^2 + 2\tilde{x}\tilde{y}(\mathbf{n}\cdot\nabla)(\boldsymbol{b}\cdot\nabla)$$
$$+ \tilde{y}^2(\boldsymbol{b}\cdot\nabla)^2] + \kappa\tilde{x}^2(\mathbf{n}\cdot\nabla)$$
$$\left.\left. + \kappa\tilde{x}\tilde{y}(\boldsymbol{b}\cdot\nabla) + \cdots\right)\right\}\frac{t(s)}{|\mathbf{x} - X(s)|}.$$ (13)

We shall see, from the inner expansion of the Euler equations in Appendix B, the following dependence of ζ on φ to second order in ϵ, the ratio of the core to curvature radii:

$$\zeta(\tilde{x},\tilde{y}) = \zeta_0 + \zeta_{11}\cos\varphi + \zeta_{12}\sin\varphi + \zeta_{21}\cos 2\varphi + \cdots,$$ (14)

where

$$\zeta_0 \approx \zeta^{(0)}(r) + \kappa^2\hat{\zeta}_0^{(2)}(r), \quad \zeta_{11} \approx \kappa\hat{\zeta}_{11}^{(1)}(r),$$

$$\zeta_{12} \approx \kappa\hat{\zeta}_{12}^{(1)}(r), \quad \zeta_{21} \approx \kappa^2\hat{\zeta}_{21}^{(2)}(r).$$ (15)

The power in κ indexes the order of the asymptotic expansion. In $\hat{\zeta}_{ij}^{(k)}$, the superscript k stands for order of expansion, and i labels the Fourier mode with $j=1$ and 2 being corresponding to $\cos i\theta$ and $\sin i\theta$, respectively. Viewed locally, we call the axisymmetric component ζ_0 the *monopole* field, $\zeta_{11}\cos\varphi$ and $\zeta_{12}\sin\varphi$ the *dipole* fields, and $\zeta_{21}\cos 2\varphi$ the *quadrupole* field. So far, the first term of (13) has exclusively received attention, which only ζ_0 takes part in. The quadrupole field is tied with the elliptical deformation of the core with a major axis along the binormal ($\boldsymbol{b}$) direction. The dipole field is tied with curvature of the vortex tube as will be explained below. In the same way as the axisymmetric problem,[16,19] the dipole functions ζ_{11} and ζ_{12} are sensitive to our choice of the origin $r=0$ of the local moving coordinates, which is noted in Appendix B. In the case of a quasisteady motion, the core shape possesses the fore-aft symmetry in the $\boldsymbol{b}$ direction. By constraining the origin on the symmetric line (the $\tilde{x}$ axis) in each core cross section, we may dispense with $\sin\varphi$ component, that is, we may take $\zeta_{12}\equiv 0$.

Retaining the first-order terms in the expansions $A_\parallel$ is sufficient to obtain a correction from finite core-area effect. By introducing $\zeta(\tilde{x},\tilde{y}) = \zeta_0 + \kappa\hat{\zeta}_{11}^{(1)}\cos\varphi$ in the expansion (13) and performing integration over the transversal or the $\tilde{x}\tilde{y}$ plane first, we are left with

$$A_\parallel(\mathbf{x}) \approx A_m(\mathbf{x}) + A_{\parallel d}(\mathbf{x}),$$ (16)

where

$$A_m(\mathbf{x}) = \frac{\Gamma}{4\pi}\int \frac{t(s)}{|\mathbf{x} - X(s)|}ds,$$ (17)

$$A_{\|d}(\mathbf{x}) = \frac{1}{8\pi} \int ds \left\{ \Gamma^{(3)} \left(\frac{1}{2} [(\mathbf{n} \cdot \nabla)^2 + (\mathbf{b} \cdot \nabla)^2] \right. \right.$$
$$\left. \left. + \kappa(\mathbf{n} \cdot \nabla) \right) - \kappa Z_{11}^{(1)} [\kappa + (\mathbf{n} \cdot \nabla)] \right\} \frac{\mathbf{t}(s)}{|\mathbf{x} - X(s)|}, \tag{18}$$

Γ is the circulation, and $\Gamma^{(3)}$ and $Z_{11}^{(1)}$ are moments of vorticity:

$$\Gamma = 2\pi \int_0^\infty r \zeta^{(0)} dr, \quad \Gamma^{(3)} = 2\pi \int_0^\infty r^3 \zeta^{(0)} dr,$$

$$Z_{11}^{(1)} = 2\pi \int_0^\infty r^2 \hat{\zeta}_{11}^{(1)} dr. \tag{19}$$

The circulation Γ is constant in both t and s, but generically this is not the case with $\Gamma^{(3)}$ and $Z_{11}^{(1)}$. The first term (17), attached with suffix m, is no other than the flow field induced by a vortex filament of infinitesimal thickness and is named the monopole field. The form of $\Gamma^{(3)}$ and $Z_{11}^{(1)}$ reveals that the correction term $A_{\|d}(\mathbf{x})$ takes account of the internal structure of the core. A further simplification of $A_{\|d}(\mathbf{x})$ is effected.

After rewriting the second derivatives as $(\mathbf{n} \cdot \nabla)^2 + (\mathbf{b} \cdot \nabla)^2 = \nabla^2 - (\mathbf{t} \cdot \nabla)^2$, we exploit

$$\nabla^2 \frac{1}{|\mathbf{x} - X(s)|} = 0 \quad \text{at } \mathbf{x} \neq X, \tag{20}$$

to it. The heart of Dyson's technique lies in canceling as many terms as possible at an early stage by a combined use of the shift operators and the harmonic nature (20), and the role of (20) in prompting cancellations cannot be overemphasized when we enter into higher orders. With the aid of

$$(\mathbf{t} \cdot \nabla) \frac{1}{|\mathbf{x} - X(s)|} = -\left(\mathbf{t} \cdot \frac{\partial}{\partial X} \right) \frac{1}{|\mathbf{x} - X(s)|} = -\frac{\partial}{\partial s} \frac{1}{|\mathbf{x} - X(s)|}, \tag{21}$$

(18) simplifies, after partial integration, to

$$A_{\|d}(\mathbf{x}) = -\frac{1}{2} \int ds \left\{ \frac{\Gamma^{(3)}}{8\pi} (\kappa_s \mathbf{n} + \kappa \tau \mathbf{b}) \right.$$
$$\left. + d^{(1)} \kappa \mathbf{t} [\kappa + (\mathbf{n} \cdot \nabla)] \right\} \frac{1}{|\mathbf{x} - X(s)|}, \tag{22}$$

where subscript s signifies the partial differentiation with respect to s and

$$d^{(1)} = \frac{1}{4\pi} \left\{ \left[2\pi \int_0^\infty r^2 \hat{\zeta}_{11}^{(1)} dr \right] - \frac{1}{2} \left[2\pi \int_0^\infty r^3 \zeta^{(0)} dr \right] \right\}. \tag{23}$$

We have assumed that the profile $\zeta^{(0)}$ is uniform in s and has ignored derivative of $\Gamma^{(3)}$ with respect to s in the process of partial integration.

The correction term $A_{\|d}$ constitutes a part of the flow field induced by *a line of dipoles*, based at the vortex center-line, with their axes oriented in the binormal direction, as will be clear from the expression (35). The coefficient $d^{(1)}$

characterizes the strength of dipole. The dipole field is a realization of curvature effect; by bending a vortex tube, the vortex lines on the convex side are stretched, while those on the concave side are contracted. As a consequence, the vorticity on the convex side is enhanced whereas that on the concave side is diminished, producing effectively a vortex pair. The velocity field induced by this antiparallel vortex pair produces the dipole field.[16,19] The expression (22), however, does not exhaust all the contribution of dipoles. The transversal vorticity should not be forgotten.

C. Contribution from transversal vorticity

Under our assumption of a quasisteady motion of a vortex filament, the components of vorticity perpendicular to $\mathbf{t}$ make its appearance at second order in ϵ. Its derivation is made in Appendix B.

The leading-order flow consists only of the local azimuthal velocity $v^{(0)}(r)$. Introduce a streamfunction

$$\psi(\mathbf{x}) = (1 - \kappa r \cos \varphi) A(\mathbf{x}) \cdot \mathbf{t}(\xi), \tag{24}$$

for the flow in the plane transversal to $\mathbf{t}$. When the terms of nonlocal origin are separated in the $O(\epsilon)$ term of ψ as (B9), the transversal components $u^{(1)}$ and $v^{(1)}$ of the relative velocity, of $O(\epsilon)$, are written in a tidy form as (B11) and (B12). As explained above, we may exclude $\hat{\psi}_{12}^{(1)}$, (B19), without loss of generality. Upon substitution from (B11) and (B12), the longitudinal vorticity (6) of $O(\epsilon)$ is reduced to (B13) and (B14), that is,

$$\zeta^{(1)} = -\kappa [\alpha \hat{\psi}_{11}^{(1)} + r \zeta^{(0)}] \cos \varphi, \tag{25}$$

where $\zeta^{(0)}$ is related to $v^{(0)}$ through (B5),

$$\alpha = \frac{1}{v^{(0)}} \frac{\partial \zeta^{(0)}}{\partial r}, \tag{26}$$

and $\hat{\psi}_{11}^{(1)}$ is the part of the first-order streamfunction proportional to $\cos \varphi$, as given by (B17) and (B18). From (4) and (5), the transversal vorticity $\boldsymbol{\omega}_\perp = \omega_r \mathbf{e}_r + \omega_\theta \mathbf{e}_\theta$, which is of $O(\epsilon^2)$, is expressible, in terms of the streamfunction, as

$$\omega_r = \hat{\omega}_r^{(2)}(r)(\kappa_s \cos \varphi + \kappa \tau \sin \varphi),$$

$$\omega_\theta = \hat{\omega}_\theta^{(2)}(r)(\kappa \tau \cos \varphi - \kappa_s \sin \varphi) - \frac{\partial w_0^{(2)}}{\partial r}, \tag{27}$$

where

$$\hat{\omega}_r^{(2)} = \frac{\zeta^{(0)}}{v^{(0)}} \hat{\psi}_{11}^{(1)}, \quad \hat{\omega}_\theta^{(2)} = \frac{r \zeta^{(0)}}{v^{(0)}} \left\{ \left[\frac{2}{r} - \frac{\zeta^{(0)}}{v^{(0)}} \right] \hat{\psi}_{11}^{(1)} \right.$$
$$\left. + \frac{\partial \hat{\psi}_{11}^{(1)}}{\partial r} - r v^{(0)} \right\}, \tag{28}$$

and use has been made of (B26) and the fact that $w^{(1)}$ is independent of r.

Since the transversal vorticity is of second order, it is enough to retain the leading term in the integrand of $A_\perp$ associated with $\boldsymbol{\omega}_\perp$ in order to supplement $A_{\|d}$. We may thus start from

$$A_\perp(\mathbf{x}) = \frac{1}{4\pi} \int \int \int \frac{\boldsymbol{\omega}_\perp(\tilde{x},\tilde{y},s)(1-\kappa\tilde{x})}{|\mathbf{x} - \mathbf{X} - \tilde{x}\mathbf{n} - \tilde{y}\mathbf{b}|} d\tilde{x} d\tilde{y} ds$$

$$\approx \frac{1}{4\pi} \int \int \int \frac{\boldsymbol{\omega}_\perp(\tilde{x},\tilde{y},s)}{|\mathbf{x} - \mathbf{X}(s)|} d\tilde{x} d\tilde{y} ds. \quad (29)$$

Integrating $\boldsymbol{\omega}_\perp$ over the transversal plane leaves

$$\int \int \boldsymbol{\omega}_\perp(\tilde{x},\tilde{y},s) d\tilde{x} d\tilde{y} \approx \left\{ \pi \int_0^\infty r[\hat{\omega}_r^{(2)} + \hat{\omega}_\theta^{(2)}] dr \right\}$$
$$\times (\kappa_s \mathbf{n} + \kappa\tau\mathbf{b}). \quad (30)$$

The representation of vorticity provided by (28) is coupled into

$$r[\hat{\omega}_r^{(2)} + \hat{\omega}_\theta^{(2)}] = -r^2[\alpha\hat{\psi}_{11}^{(1)} + r\zeta^{(0)}] + \frac{d}{dr}\left[\frac{r^2\zeta^{(0)}}{v^{(0)}} \hat{\psi}_{11}^{(1)} \right]. \quad (31)$$

Since $\hat{\zeta}_{11}^{(1)} = -[\alpha\hat{\psi}_{11}^{(1)} + r\zeta^{(0)}]$, as given by (25), integration in (30) is written in terms of $\hat{\zeta}_{11}^{(1)}$, and (29) is reduced to

$$A_\perp \approx \frac{1}{8\pi} \int Z_{11}^{(1)} \frac{\kappa_s(s)\mathbf{n}(s) + \kappa(s)\tau(s)\mathbf{b}(s)}{|\mathbf{x} - \mathbf{X}(s)|} ds. \quad (32)$$

This is the dipole field originating from the transversal vorticity. Summation of (22) and (32) gives rise to

$$A_d(\mathbf{x}) = \frac{1}{2} \int ds\, d^{(1)}(s)\{\kappa_s\mathbf{n} + \kappa\tau\mathbf{b} - \kappa t[\kappa$$
$$+ (\mathbf{n} \cdot \nabla)]\} \frac{1}{|\mathbf{x} - \mathbf{X}(s)|}. \quad (33)$$

The assumption made so far is that Γ and $\Gamma^{(3)}$ are uniform along the tube. Suppose further that $Z_{11}^{(1)}$ is independent of s and therefore that so is $d^{(1)}$. With the help of $(\kappa\mathbf{n})_s = \kappa_s\mathbf{n} + \kappa\tau\mathbf{b} - \kappa^2\mathbf{t}$, this is further simplified by partial integration. Together with the monopole field (17), we arrive at the first two terms of the multipole expansion as

$$A(\mathbf{x}) \approx \frac{\Gamma}{4\pi} \int \frac{\mathbf{t}(s)}{|\mathbf{x} - \mathbf{X}(s)|} ds$$
$$- \frac{d^{(1)}}{2} \int \frac{\kappa(s)\mathbf{b}(s) \times [\mathbf{x} - \mathbf{X}(s)]}{|\mathbf{x} - \mathbf{X}(s)|^3} ds. \quad (34)$$

A physical meaning is brought out by taking the curl of (34),

$$\mathbf{u}(\mathbf{x}) \approx -\frac{\Gamma}{4\pi} \int \frac{[\mathbf{x} - \mathbf{X}(s)] \times \mathbf{t}(s)}{|\mathbf{x} - \mathbf{X}(s)|^3} ds + \frac{d^{(1)}}{2} \int \kappa(s)$$
$$\times \left\{ \frac{\mathbf{b}(s)}{|\mathbf{x} - \mathbf{X}(s)|^3} - \frac{3\mathbf{b}(s) \cdot [\mathbf{x} - \mathbf{X}(s)]}{|\mathbf{x} - \mathbf{X}(s)|^5} [\mathbf{x} - \mathbf{X}(s)] \right\} ds. \quad (35)$$

Plainly, the second integral signifies the induced velocity by a collection of dipoles distributed on the tube centerline. The dipole is oriented in the local $\mathbf{b}$ direction and its strength is $d^{(1)}\kappa(s)/2$, being indicative of curvature origin.

With the help of Dyson's technique, it is rather straightforward to advance the expansion to next order. The induction velocity due to a line of quadrupoles, associated with the elliptical deformation of core cross section, comes out. This term is necessary to gain the self-induced speed of the helical tube, but we may dispense with it for the present purpose.

D. Examples

To have an idea of the dipoles, we evaluate its strength $d^{(1)}$ for typical examples. We pick out uniform and Gaussian distributions of vorticity at $O(\epsilon^0)$.

The Rankine vortex has the uniform vorticity distribution in the circular core of radius σ. We keep the origin $r=0$ of the local moving coordinates sitting at the center of the circle. This amounts to choosing $c_{11}^{(1)} = -5\sigma^2/8$ and $c_{12}^{(1)} = 0$ in (B17).[16] In dimensional form, the leading-order field is given by

$$\zeta^{(0)} = \begin{cases} \dfrac{\Gamma}{\pi\sigma^2} \\ 0, \end{cases} \qquad v^{(0)} = \begin{cases} \dfrac{\Gamma}{2\pi\sigma^2} r & (r \leqslant \sigma) \\ \dfrac{\Gamma}{2\pi r} & (r > \sigma). \end{cases} \quad (36)$$

The first-order vorticity takes the form of $\zeta^{(1)} = \kappa\hat{\zeta}_{11}^{(1)} \cos\varphi$. In (B14), $\alpha = -(2/\sigma)\delta(r-\sigma)$ and $\alpha\hat{\psi}_{11}^{(1)} = 0$, concomitant with the choice of the coordinate origin,[16,19] and we have directly from (B14), (B17), and (B18), upon introduction of (36),

$$\hat{\zeta}_{11}^{(1)} = \begin{cases} -\dfrac{\Gamma}{\pi\sigma^2} r & (r \leqslant \sigma) \\ 0 & (r > \sigma). \end{cases} \quad (37)$$

The linear dependence on r inherits from the exact relation that the vorticity is proportional to ρ, the distance from the axis of symmetry. Inserting (36) and (37) into (23), we have

$$d^{(1)} = -\frac{3}{16\pi}\Gamma\sigma^2. \quad (38)$$

Alternatively, with the choice of $c_{11}^{(1)} = c_{12}^{(1)} = 0$, the origin $r=0$ is maintained at the stagnation point, in the transversal plane, viewed from the coordinate frame moving with the vortex tube. The line of these points coincides, to $O(\epsilon^2)$, with the local minimum line of the pressure, and hence is liable to be visualized as a cavitation line.[19] With this choice, the dipole strength is modified as $d^{(1)} = 1/(8\pi)\Gamma\sigma^2$. Note that even the sign differs from (38).

Next we turn to the Gaussian distribution of vorticity, a more realistic one. The leading-order vorticity is

$$\zeta^{(0)} = \frac{\Gamma}{\pi\sigma^2} e^{-r^2/\sigma^2}, \quad (39)$$

and the corresponding azimuthal velocity is

$$v^{(0)} = \frac{\Gamma}{2\pi r}(1 - e^{-r^2/\sigma^2}). \quad (40)$$

Notably, the Gaussian distribution is compatible with the Navier-Stokes equations. The kinematic viscosity ν selects $\sigma^2 = 4\nu t$ for a vortex ring starting from an infinitely thin core at $t=0$.[17–19] For a continuous distribution of the core, the form center of the circular core is hard to be identified. A natural choice, of physical significance, is to take $r=0$ on the

relative stagnation line by putting $c_{11}^{(1)}=c_{12}^{(1)}=0$. Then the radial function of the first-order streamfunction consists of $\hat{\Psi}_{11}^{(1)}$, defined by (B18), alone. The dipole strength $d^{(1)}$ is found from the asymptotic behavior of (B20) of $\hat{\Psi}_{11}^{(1)}$, valid at large distances ($\sigma \ll r \ll 1/\kappa$), and, by l'Hospital's rule, we deduce

$$\frac{d^{(1)}}{\Gamma \sigma^2} = \frac{1}{8\pi} \lim_{r \to \infty} \left\{ \int_0^{r^2} \frac{dx'}{(1-e^{-x'})^2} \int_0^{x'} \frac{(1-e^{-x''})^2}{x''} dx'' \right.$$

$$\left. - r^2 [2 \log r + \gamma - \log 2 - 1] \right\}$$

$$\approx 0.103\,063\,722\,778, \tag{41}$$

where $\gamma \approx 0.577\,215\,664\,902$ is Euler's constant.

An alternative choice of the origin $r=0$ is the line of the local maximum vorticity, and this is attained by the choice of $c_{11}^{(1)} = \sigma^2/2$.[19] This line is also detectable by an experimental measurement of velocity field or by an analysis of numerical data of a computer simulation. In this case, the factor of (41) is increased to 0.182 641 194 324.

III. VELOCITY FIELD INDUCED BY A HELICAL MONOPOLE FILAMENT

A helical vortex is an elementary vortical structure featured by having torsion, in addition to curvature. We are tempted to look into the influence of finite-core size on the velocity around a helical vortex tube by applying the result of the preceding section. Before that, we are reminded of the velocity field induced by an infinitely thin helical vortex filament for introducing notations and for reference later. Many of asymptotic expansions[6–8] have been built on the footing of the Kapteyn series obtained by Hardin,[1] which we shall follow.

A. Helix geometry

Consider the flow induced by an infinitely thin helical vortex filament of strength Γ embedded in an unbounded fluid. Setting the pitch as $2\pi l$ and the radius of the supporting cylinder as a, the filament curve $\mathbf{x}'(\phi) = [x'(\phi), y'(\phi), z'(\phi)]$ is represented by

$$x' = a \cos \phi, \quad y' = a \sin \phi, \quad z' = l\phi, \tag{42}$$

as illustrated in Fig. 2. The parameter ϕ has a link with the arc-length parameter via $ds = d\phi \sqrt{a^2+l^2}$. The triad of orthonormal unit vectors, the tangent, the normal, and the binormal vectors $\mathbf{t}$, $\mathbf{n}$ and $\mathbf{b}$, at each point on the filament is expressed by

$$\mathbf{t} = \frac{a}{\sqrt{a^2+l^2}} \left(-\sin\phi, \cos\phi, \frac{l}{a} \right),$$

$$\mathbf{n} = (-\cos\phi, -\sin\phi, 0),$$

$$\mathbf{b} = \frac{l}{\sqrt{a^2+l^2}} \left(\sin\phi, -\cos\phi, \frac{a}{l} \right), \tag{43}$$

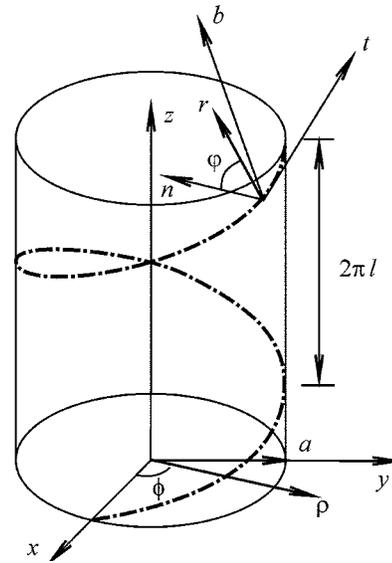and the curvature κ and the torsion τ are given by

FIG. 2. Coordinate system and sketch of the center line of a helical vortex tube.

$$\kappa = \frac{a}{a^2+l^2}, \quad \tau = \frac{l}{a^2+l^2}. \tag{44}$$

B. Vector potential

At the outset, we write, at a general position $\mathbf{x} = (\rho \cos \phi, \rho \sin \phi, z)$, the vector potential $\mathbf{A}_m(\mathbf{x})$ given by (17) or the first term of (34), associated with the monopoles on the uniform helix (42), in the Kapteyn series. Actually, the streamfunction of a helically symmetric flow, treated by Hardin,[1] inherits from this.

We borrow Hardin's notation

$$I(\alpha, r) = \int_{-\infty}^{\infty} \frac{\exp(i\alpha\theta)}{r} d\theta, \tag{45}$$

where $r = [\rho^2 + a^2 - 2a\rho \cos(\phi-\theta) + (z-l\theta)^2]^{1/2}$ is the distance of $\mathbf{x}$ from $\mathbf{x}'(\theta)$. To shorten the resulting expressions, we define

$$\chi = \phi - z/l, \tag{46}$$

and introduce the notation

$$H_M^{I,J}(x,y,\chi) = \sum_{m=1}^{\infty} m^M I_m^{\langle I \rangle}(mx) K_m^{\langle J \rangle}(my) e^{im\chi}, \tag{47}$$

constituted from products $I_m(\cdot)$ and $K_m(\cdot)$, the modified Bessel functions of the first and second kinds of the mth order. The superscript $\langle I \rangle$ designates the Ith derivative with respect to its argument with $\langle 0 \rangle$ for the function itself. The cylindrical components ($A_{m\rho}$, $A_{m\phi}$, and A_{mz}) of $\mathbf{A}_m$ at $\mathbf{x}$ are then written as

$$A_{m\rho} = \frac{\Gamma a}{4\pi} \mathrm{Re}[ie^{-i\phi}I(1,r)]$$

$$= -\frac{\Gamma a}{\pi l} \mathrm{Im}\left[\frac{l}{\rho}\left\{\begin{matrix}H_0^{0,1}(\rho/l,a/l,\chi)\\H_0^{1,0}(a/l,\rho/l,\chi)\end{matrix}\right\} + \frac{l}{a}\left\{\begin{matrix}H_0^{1,0}(\rho/l,a/l,\chi)\\H_0^{0,1}(a/l,\rho/l,\chi)\end{matrix}\right\}\right], \tag{48}$$

$$A_{m\phi} = \frac{\Gamma a}{4\pi} \mathrm{Im}[ie^{-i\phi}I(1,r)]$$

$$= \frac{\Gamma a}{4\pi l}\left\{\begin{matrix}\rho/a\\a/\rho\end{matrix}\right\} - \frac{\Gamma a}{\pi l} \mathrm{Re}\left[\left\{\begin{matrix}H_0^{1,1}(\rho/l,a/l,\chi)\\H_0^{1,1}(a/l,\rho/l,\chi)\end{matrix}\right\} + \frac{l^2}{\rho a}\left\{\begin{matrix}H_0^{0,0}(\rho/l,a/l,\chi)\\H_0^{0,0}(a/l,\rho/l,\chi)\end{matrix}\right\}\right], \tag{49}$$

$$A_{mz} = \frac{\Gamma l}{4\pi}I(0,r)$$

$$= -\frac{\Gamma}{2\pi}\left\{\begin{matrix}\log a\\\log \rho\end{matrix}\right\} + \frac{\Gamma}{\pi} \mathrm{Re}\left\{\begin{matrix}H_0^{0,0}(\rho/l,a/l,\chi)\\H_0^{0,0}(a/l,\rho/l,\chi)\end{matrix}\right\}, \tag{50}$$

where $\mathrm{Re}[\cdot]$ and $\mathrm{Im}[\cdot]$ indicate the real and imaginary parts, respectively. Here and hereinafter the top line in braces corresponds to the expression for $\rho < a$, and the bottom one to that for $\rho > a$. In the last equation (50), an indefinite constant has been dropped off as this parameter is inconsequential for the velocity field obtained by taking its curl.

C. Streamfunction

Notice that the vector potential (48)–(50) depends only upon two variables ρ and χ, being indicative of helical symmetry. In this keeping, the helical symmetry imposes the constraint that the velocity component tangent to helical lines of pitch $2\pi l$ is constant globally in space,

$$u_\tau = u_z + \frac{\rho}{l}u_\phi = \mathrm{const}. \tag{51}$$

The fluid flow with helical symmetry may be taken as a two-dimensional flow with uniform "translation motion" along the helical lines. Consequently, by introducing the velocity component orthogonal both to e_ρ and e_τ,

$$u_\chi = u_\phi - \frac{\rho}{l}u_z, \tag{52}$$

the velocity field of this virtually two-dimensional flow is expressible solely by a single function Ψ as[1]

$$u_\rho = \frac{1}{\rho}\frac{\partial\Psi}{\partial\chi}, \quad u_\chi = -\frac{\partial\Psi}{\partial\rho}. \tag{53}$$

This streamfunction is coined by a superposition of components of the vector potential:

$$\Psi = A_z + \frac{\rho}{l}A_\phi. \tag{54}$$

Combination of (49) and (50) gives the streamfunction Ψ_m for the monopole field, up to an indefinite constant, as

$$\Psi_m = \frac{\Gamma}{4\pi}\left\{\begin{matrix}\rho^2/l^2 - \log(a^2)\\a^2/l^2 - \log(\rho^2)\end{matrix}\right\} - \frac{\Gamma a\rho}{\pi l^2} \mathrm{Re}\left\{\begin{matrix}H_0^{1,1}(\rho/l,a/l,\chi)\\H_0^{1,1}(a/l,\rho/l,\chi)\end{matrix}\right\}. \tag{55}$$

Hardin's solution[1] entails a discontinuity in ρ across $\rho=a$. He obtained the streamfunction via integration of the velocity field. Continuous matching has been achieved by relying upon the vector potential as (54).

The representation of streamfunction in an infinite series $H_M^{I,J}$ is a generalization of the well-known Kapteyn series.[27] Note that convergence of the series $H_M^{I,J}(x,y,\chi)$ becomes deteriorated as x approaches y (see Appendix C), which stands as an obstacle for calculating the near field. A method has been developed to separate dominant singular behavior in the series (47) by an introduction of strained spatial variables that take the filament torsion into consideration (see Appendix C).[9,22] Unlike other methods,[8,28] this approach utilizes solely elementary functions to represent, with a quite high accuracy, the flow field at any point.

Substituting the singularity-separation form (C3) into $H_M^{I,J}$ and using the symmetrical properties of $\lambda^{I,J}$, $\alpha^{I,J}$, and $\beta^{I,J}$, for instance, $\lambda^{1,1}(x,y)=\lambda^{1,1}(y,x)$ and $\alpha^{1,1}(x,y)=-\alpha^{1,1}(y,x)$, etc., Ψ_m is rearranged as

$$\Psi_m = \frac{\Gamma}{4\pi}\left\{\begin{matrix}\rho^2/l^2 - \log(a^2)\\a^2/l^2 - \log(\rho^2)\end{matrix}\right\} - \frac{\Gamma a\rho}{\pi l^2}\lambda^{1,1} \mathrm{Re}[\log(1 - e^{\pm\xi+i\chi})$$
$$\pm \alpha^{1,1}\mathrm{Li}_2(e^{\pm\xi+i\chi}) + \beta^{1,1}\mathrm{Li}_3(e^{\pm\xi+i\chi})]$$
$$- \frac{\Gamma a\rho}{\pi l^2} \mathrm{Re}\left\{\begin{matrix}R_0^{1,1}(\rho/l,a/l,\chi)\\R_0^{1,1}(a/l,\rho/l,\chi)\end{matrix}\right\}, \tag{56}$$

where $\mathrm{Li}_2(\cdot)$ and $\mathrm{Li}_3(\cdot)$ are the polylogarithms defined by (C2), and $\lambda^{1,1}$, $\alpha^{1,1}$, and $\beta^{1,1}$ are functions of ρ made, respectively, from (C5), (C7), and (C8) in Appendix C via

$$\lambda^{I,J} = \lambda^{I,J}(\rho/l,a/l), \quad \alpha^{I,J} = \alpha^{I,J}(\rho/l,a/l),$$

$$\beta^{I,J} = \beta^{I,J}(\rho/l,a/l). \tag{57}$$

The remainder $R_0^{1,1}$ is defined by (C12). Hereinafter in double sign notation ("$\pm$" or "$\mp$"), the upper sign corresponds to $\rho < a$, and the lower to $\rho > a$. The distorted variable ξ is defined in exponential form by

$$e^\xi = \frac{\rho'}{a'} = \frac{\rho}{a}\frac{(l + \sqrt{l^2 + a^2})\exp(\sqrt{l^2 + \rho^2})}{(l + \sqrt{l^2 + \rho^2})\exp(\sqrt{l^2 + a^2})}. \tag{58}$$

The transformed coordinate $\rho' = \rho\exp(\sqrt{l^2+\rho^2})/(l+\sqrt{l^2+\rho^2})$ may be thought of as the radial coordinate in the distorted space. If we take the limit of $l \to \infty$, or the helical filament straightens, the limiting form of (56) approaches the streamfunction for a rectilinear vortex filament.

The representation (56) is formally exact but, for practical applications, it is enough to single out the first two terms. After some manipulation of the coefficients $\lambda^{1,1}$, $\alpha^{1,1}$, and $\beta^{1,1}$, we produce a rough-and-ready formula as
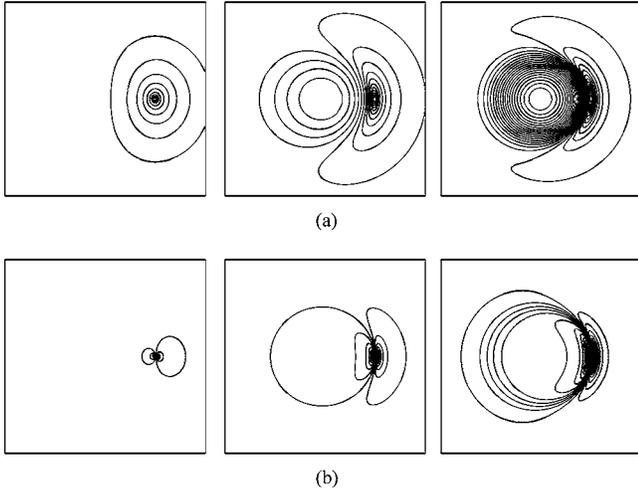
(a)

(b)

FIG. 3. Isolines of the streamfunctions of a helical filament of (a) monopoles and (b) dipoles for different values of dimensionless pitch $h=2\pi l/a$ $=8$, 2, and 1 from left to right. The normalized strength of dipole is $d/(\Gamma a)=-0.05$. The separation value between neighboring contours is $\Delta\Psi/\Gamma=1/\pi$.

$$\Psi_m \approx \frac{\Gamma}{4\pi}\left\{ \begin{array}{c} \rho^2/l^2 - \log(a^2) \\ a^2/l^2 - \log(\rho^2) \end{array} \right\}$$

$$+ \frac{\Gamma}{2\pi l}\sqrt[4]{(l^2+\rho^2)(l^2+a^2)}\ \mathrm{Re}[\log(1 - e^{\pm\xi+i\chi})]$$

$$\pm \frac{\Gamma}{48\pi}\sqrt[4]{(l^2+\rho^2)(l^2+a^2)}\left[\frac{2l^2+9a^2}{(l^2+a^2)^{3/2}} \right.$$

$$\left. -\frac{2l^2+9\rho^2}{(l^2+\rho^2)^{3/2}}\right]\mathrm{Re}[\mathrm{Li}_2(e^{\pm\xi+i\chi})]. \tag{59}$$

As will be demonstrated in Appendix C, numerical error of (59), the two-term truncation, is no more than 3% and this discrepancy is indiscernible in graphical plots. For this reason, all flow characteristics may be captured well on the basis of the rough-and-ready formulas. Figure 3(a) illustrates the variation of the contours $\Psi_m=\mathrm{const}$ with normalized helical pitch $h=2\pi l/a$, with the common contour step $\Delta\Psi_m/\Gamma=1/\pi$ throughout the cases of $h=1$, 2, and 8. At a large pitch, the streamfunction looks like that for a straight vortex filament, with small deformation of the isolines from circles. As the pitch is decreased, a substantial change in contours appears inside the wound cylinder $(\rho<a)$ and the contours adjacent to the filament, on which the monopoles are sitting, deforms into crescent form. The velocity field is informative for an understanding of this deformation, as will be worked out subsequently.

D. Velocity field

The velocity field $\mathbf{u}_m=(u_\rho, u_\phi, u_z)$ induced by a line of monopole singularity on the helical filament is calculated from the formula $\mathbf{u}_m=\nabla\times\mathbf{A}_m$. Taking the curl of (48)–(50), we have

$$u_\rho = \frac{\Gamma a}{\pi l^2}\ \mathrm{Im}\left\{ \begin{array}{c} H_1^{1,1}(\rho/l, a/l, \chi) \\ H_1^{1,1}(a/l, \rho/l, \chi) \end{array} \right\}, \tag{60}$$

$$u_z = \frac{\Gamma}{2\pi l}\left\{ \begin{array}{c} 1 \\ 0 \end{array} \right\} - \frac{\Gamma a}{\pi l^2}\ \mathrm{Re}\left\{ \begin{array}{c} H_1^{0,1}(\rho/l, a/l, \chi) \\ H_1^{1,0}(a/l, \rho/l, \chi) \end{array} \right\}. \tag{61}$$

The azimuthal component u_ϕ is found from

$$u_\phi = \frac{\Gamma}{2\pi\rho} - \frac{lu_z}{\rho}. \tag{62}$$

These formulas apply to the velocity field induced by a right-handed helical filament. To adapt to a left-handed helix, it suffices to reverse the signs of u_z and to put $\chi=\phi+z/l$ instead of (46). The same formulas are reached by way of (53) with Ψ provided by (55). The constant in (51) is $\Gamma/2\pi l$.

In the same manner as for the streamfunction, the partial sum of dominant terms in the Kapteyn series can be carried out for the velocity, which is corrected by the less singular remainder terms. The resulting representations are

$$u_\rho = \frac{\Gamma a}{\pi l^2}\lambda^{1,1}\ \mathrm{Im}\left[\frac{e^{i\chi}}{e^{\mp\xi}-e^{i\chi}} \pm \alpha^{1,1}\log(1-e^{\pm\xi+i\chi})\right.$$

$$\left. + \beta^{1,1}\mathrm{Li}_2(e^{\pm\xi+i\chi}) \pm \gamma^{1,1}\mathrm{Li}_3(e^{\pm\xi+i\chi})\right]$$

$$+ \frac{\Gamma a}{\pi l^2}\ \mathrm{Im}\left\{ \begin{array}{c} R_1^{1,1}(\rho/l, a/l, \chi) \\ R_1^{1,1}(a/l, \rho/l, \chi) \end{array} \right\}, \tag{63}$$

$$u_z = \frac{\Gamma}{2\pi l}\left\{ \begin{array}{c} 1 \\ 0 \end{array} \right\} - \frac{\Gamma a}{\pi l^2}\lambda^{0,1}\ \mathrm{Re}\left[\frac{\pm e^{i\chi}}{e^{\mp\xi}-e^{i\chi}} + \alpha^{0,1}\log(1\right.$$

$$\left. -e^{\pm\xi+i\chi}) \pm \beta^{0,1}\mathrm{Li}_2(e^{\pm\xi+i\chi}) + \gamma^{0,1}\mathrm{Li}_3(e^{\pm\xi+i\chi})\right]$$

$$+ \frac{\Gamma a}{\pi l^2}\ \mathrm{Re}\left\{ \begin{array}{c} R_1^{0,1}(\rho/l, a/l, \chi) \\ R_1^{1,0}(a/l, \rho/l, \chi) \end{array} \right\}, \tag{64}$$

where we have defined, using (C9),

$$\gamma^{J,J} = \gamma^{J,J}(\rho/l, a/l), \tag{65}$$

and $\lambda^{0,1}$, $\alpha^{0,1}$, and $\beta^{0,1}$ are functions given by (57). The exponential term e^ξ is given by (58), and the detailed form of the remainders $R_1^{1,1}$, $R_1^{0,1}$, and $R_1^{1,0}$ is defined in Appendix C.

When the dominant first two terms are extracted, they are reduced to

$$u_\rho \approx -\frac{\Gamma}{2\pi\rho l}\sqrt[4]{(l^2+\rho^2)(l^2+a^2)}\ \mathrm{Im}\left\{\frac{e^{i\chi}}{e^{\mp\xi}-e^{i\chi}}\right.$$

$$\pm \frac{l}{24}\left[\frac{2l^2+9a^2}{(l^2+a^2)^{3/2}}\right.$$

$$\left.\left. -\frac{2l^2+9\rho^2}{(l^2+\rho^2)^{3/2}}\right]\log(1-e^{\pm\xi+i\chi})\right\}, \tag{66}$$

$$u_z \approx \frac{\Gamma}{2\pi l}\left\{ \begin{array}{c} 1 \\ 0 \end{array} \right\} + \frac{\Gamma}{2\pi l}\frac{\sqrt[4]{l^2+a^2}}{\sqrt[4]{l^2+\rho^2}}\ \mathrm{Re}\left\{\frac{\pm e^{i\chi}}{e^{\mp\xi}-e^{i\chi}}\right.$$

$$\left. + \frac{l}{24}\left[\frac{3\rho^2-2l^2}{(l^2+\rho^2)^{3/2}} + \frac{9a^2+2l^2}{(l^2+a^2)^{3/2}}\right]\log(1-e^{\xi+i\chi})\right\}. \tag{67}$$
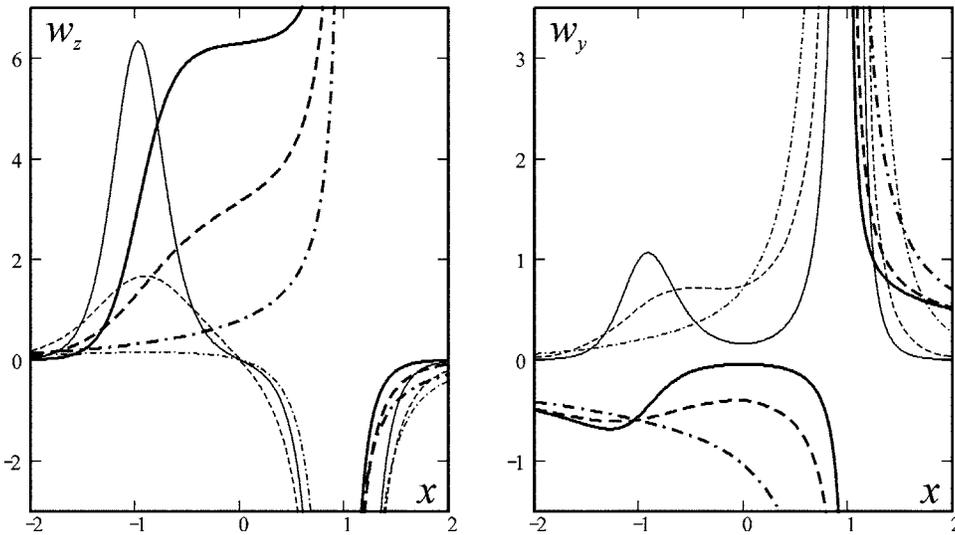
FIG. 4. Axial ($w_z = u_z$ or v_z) and azimuthal ($w_\phi = u_\phi$ or v_ϕ; $w_y = -w_\phi$ for $x < 0$ and $w_y = w_\phi$ for $x \geq 0$) velocity profiles, along the Ox axis at $z=0$, of a helical filament of monopoles (thick lines) and of dipoles (thin lines), of strength $d/(\Gamma a) = -0.05$, for different values of normalized pitch: $h=1$ (solid lines), 2 (dashed lines), and 8 (dash-dotted lines). The velocity is normalized by $\Gamma/(2\pi a)$ and the horizontal axis is x/a, or equivalently $\Gamma = 2\pi$ and $a=1$.

The thick lines on Fig. 4 draw the axial and azimuthal velocity profiles, calculated from (67) and (62), for flows induced by the monopole filament of $h=1$, 2, and 8. At a large pitch, the velocity profile does not differ very much from that of a straight vortex filament, except for small asymmetrical deformation. For a helical filament of small pitch, an intense axial flow is driven inside the supporting cylinder ($\rho < a$), but instead rotational motion subsides down there. A monopole helical filament of small pitch induces an intense jet-like fluid motion without rotation inside the cylinder, whereas fluid rotation of symmetric form, without axial motion, takes place outside of the cylinder.

IV. VELOCITY FIELD INDUCED BY A HELICAL DIPOLE FILAMENT

In this section we turn our attention to the flow induced by a line of dipole singularities on a helical filament, arising from the coupling effect of finite-core thickness and center-line curvature. This flow furnishes the dominant correction to the monopole induction considered in Sec. III, but has so far been untouched.

A. Vector potential

Let us introduce the vector potential D for the second term A_d of (34), namely, $A_d = \nabla \times D$. This definition reads

$$D(\mathbf{x}) = -\int \frac{\mathbf{d}(s)}{|\mathbf{x} - \mathbf{x}'(s)|} ds, \quad (68)$$

along with

$$\mathbf{d} = \frac{1}{2} d^{(1)} \kappa \mathbf{b}. \quad (69)$$

The dipole strength $d^{(1)}$ of $O(\epsilon)$ depends upon the vorticity distribution as is read from (23).

Noting from (43) that $\mathbf{d}(s) ds = d(l \sin \phi, -l \cos \phi, a) d\phi$ with $d = |\mathbf{d}| = d^{(1)} \kappa/2$, the cylindrical components of D are expressed by constant multiples of the components (48)–(50) as

$$D = d\{l \operatorname{Re}[ie^{-i\phi} I(1,r)], l \operatorname{Im}[ie^{-i\phi} I(1,r)], -aI(0,r)\}$$

$$= \frac{4\pi dl}{\Gamma a}\left(A_{m\rho}, A_{m\phi}, -\frac{a^2}{l^2} A_{mz}\right). \quad (70)$$

The curl of (70) leads to

$$A_{d\rho} = \frac{4d}{l} \operatorname{Im}\left[\begin{Bmatrix} H_1^{1,1}(\rho/l, a/l, \chi) \\ H_1^{1,1}(a/l, \rho/l, \chi) \end{Bmatrix} + \frac{a^2 + l^2}{\rho a}\begin{Bmatrix} H_1^{0,0}(\rho/l, a/l, \chi) \\ H_1^{0,0}(a/l, \rho/l, \chi) \end{Bmatrix}\right], \quad (71)$$

$$A_{d\phi} = -\frac{2d}{l}\begin{Bmatrix} 0 \\ a/\rho \end{Bmatrix} + 4d \operatorname{Re}\left[\frac{1}{\rho}\begin{Bmatrix} H_1^{0,1}(\rho/l, a/l, \chi) \\ H_1^{1,0}(a/l, \rho/l, \chi) \end{Bmatrix} + \frac{a^2 + l^2}{al^2}\begin{Bmatrix} H_1^{1,0}(\rho/l, a/l, \chi) \\ H_1^{0,1}(a/l, \rho/l, \chi) \end{Bmatrix}\right], \quad (72)$$

$$A_{dz} = 2d\begin{Bmatrix} 1/a \\ 0 \end{Bmatrix} - \frac{4d}{l}\operatorname{Re}\begin{Bmatrix} H_1^{0,1}(\rho/l, a/l, \chi) \\ H_1^{1,0}(a/l, \rho/l, \chi) \end{Bmatrix}, \quad (73)$$

where χ is defined by (46).

B. Streamfunction

In parallel with (54) for the monopole induction, we can introduce the streamfunction Ψ_d associated with the dipole induction. Substitution from (72) and (73) yields

$$\Psi_d = A_{dz} + \frac{\rho}{l} A_{d\phi} = \frac{2d}{l}\begin{Bmatrix} l/a \\ -a/l \end{Bmatrix} + \frac{4d\rho(a^2 + l^2)}{al^3} \operatorname{Re}\begin{Bmatrix} H_1^{1,0}(\rho/l, a/l, \chi) \\ H_1^{0,1}(a/l, \rho/l, \chi) \end{Bmatrix}. \quad (74)$$

With the help of the formulas in Appendix C, we can afford to perform an infinite summation of dominant contributions and thereby deduce a representation with separation of the singularities as

$$\Psi_d = \frac{2d}{l}\left\{\begin{matrix} l/a \\ -a/l \end{matrix}\right\} + \frac{4d\rho(a^2+l^2)}{al^3}\lambda^{1,0}\,\mathrm{Re}\left[\frac{\pm e^{i\chi}}{e^{\mp\xi}-e^{i\chi}}\right.$$

$$+\,\alpha^{1,0}\log(1-e^{\pm\xi+i\chi})\pm\beta^{1,0}\mathrm{Li}_2(e^{\pm\xi+i\chi})$$

$$\left.+\,\gamma^{1,0}\mathrm{Li}_3(e^{\pm\xi+i\chi})\right]$$

$$+\frac{4d\rho(a^2+l^2)}{al^3}\,\mathrm{Re}\left\{\begin{matrix} R_1^{1,0}(\rho/l,a/l,\chi) \\ R_1^{0,1}(a/l,\rho/l,\chi) \end{matrix}\right\}, \tag{75}$$

where for the coefficients $\lambda^{1,0}$, $\alpha^{1,0}$, $\beta^{1,0}$, and $\gamma^{1,0}$ and remainders $R_1^{1,0}$ and $R_1^{0,1}$, (57) and (65), and Appendix C should be consulted. The definition of the exponential term e^ξ is given by (58). A further simplification is achieved by retaining only the first two singular terms, leaving

$$\Psi_d \approx \frac{2d}{l}\left\{\begin{matrix} l/a \\ -a/l \end{matrix}\right\}$$

$$+\frac{2d}{al^2}(l^2+a^2)^{3/4}\sqrt[4]{l^2+\rho^2}\,\mathrm{Re}\left[\frac{\pm e^{i\chi}}{e^{\mp\xi}-e^{i\chi}}\right]$$

$$+\frac{d}{12al}(l^2+a^2)^{3/4}\sqrt[4]{l^2+\rho^2}\left[\frac{2l^2-3a^2}{(l^2+a^2)^{3/2}}\right.$$

$$\left.-\frac{9\rho^2+2l^2}{(l^2+\rho^2)^{3/2}}\right]\mathrm{Re}[\log(1-e^{\pm\xi+i\chi})]. \tag{76}$$

As scrutinized in Appendix C, the rough-and-ready formula (76) produces the values of the streamfunction, over the entire spatial range, within an accuracy of 3%. In Fig. 3(b), isolines Ψ_d=const are compared with the monopole streamlines Ψ_m=const of Fig. 3(a), for the same values of dimensionless helical pitch (h=8, 2, and 1). We choose $d/(\Gamma a)=-0.05$ for the strength of dipole filament. The separation value between neighboring isolines is Γ/π in common with the monopole case. The structure of the dipole singularity is clearly recognized. As the pitch is decreased, a drastic change in the flow pattern arises near the point of dipole singularity. At a small value of pitch, highly deformed streamlines are confined to two crescent regions, emanating from the dipole, one inside and the other outside the supporting cylinder.

C. Velocity field

The components of the velocity field $\mathbf{u}_d=(v_\rho,v_\phi,v_z)=\nabla\times\boldsymbol{A}_d$ is found from (71)–(73) in a straightforward manner as

$$v_\rho = -4d\frac{a^2+l^2}{al^3}\,\mathrm{Im}\left\{\begin{matrix} H_2^{1,0}(\rho/l,a/l,\chi) \\ H_2^{0,1}(a/l,\rho/l,\chi) \end{matrix}\right\}, \tag{77}$$

$$v_z = 4d\frac{a^2+l^2}{al^3}\,\mathrm{Re}\left\{\begin{matrix} H_2^{0,0}(\rho/l,a/l,\chi) \\ H_2^{0,0}(a/l,\rho/l,\chi) \end{matrix}\right\}. \tag{78}$$

The remaining component v_ϕ is found from

$$v_z + \rho v_\phi/l = 0, \tag{79}$$

meaning that the velocity component (51) tangent to the helices of pitch $2\pi l$ is absent. The velocity component (52),

orthogonal both to the tangent to the helices and the radial directions, is present. The effectively two-dimensional velocity field (v_ρ,v_χ) is built via (53) with Ψ substituted from (74).

The singularity-separation form of the velocity field is written in its exact form as

$$v_\rho = -4d\frac{a^2+l^2}{al^3}\lambda^{1,0}\,\mathrm{Im}\left[\frac{\pm e^{\mp\xi+i\chi}}{(e^{\mp\xi}-e^{i\chi})^2}\right.$$

$$+\,\alpha^{1,0}\frac{e^{i\chi}}{e^{\mp\xi}-e^{i\chi}}\pm\beta^{1,0}\log(1-e^{\pm\xi+i\chi})$$

$$\left.+\,\gamma^{1,0}\mathrm{Li}_2(e^{\pm\xi+i\chi})\right]-4d\frac{a^2+l^2}{al^3}\,\mathrm{Im}\left\{\begin{matrix} R_2^{1,0}(\rho/l,a/l,\chi) \\ R_2^{0,1}(a/l,\rho/l,\chi) \end{matrix}\right\}, \tag{80}$$

$$v_z = 4d\frac{a^2+l^2}{al^3}\lambda^{0,0}\,\mathrm{Re}\left[\frac{e^{\mp\xi+i\chi}}{(e^{\mp\xi}-e^{i\chi})^2}\pm\alpha^{0,0}\frac{e^{i\chi}}{e^{\mp\xi}-e^{i\chi}}\right.$$

$$\left.+\,\beta^{0,0}\log(1-e^{\pm\xi+i\chi})\pm\gamma^{0,0}\mathrm{Li}_2(e^{\pm\xi+i\chi})\right]$$

$$+4d\frac{a^2+l^2}{al^3}\mathrm{Re}\left\{\begin{matrix} R_2^{0,0}(\rho/l,a/l,\chi) \\ R_2^{0,0}(a/l,\rho/l,\chi) \end{matrix}\right\}, \tag{81}$$

and their neat approximation is

$$v_\rho \approx -\frac{2d}{a\rho l^2}(l^2+a^2)^{3/4}\sqrt[4]{l^2+\rho^2}\,\mathrm{Im}\left\{\frac{\pm e^{\mp\xi+i\chi}}{(e^{\mp\xi}-e^{i\chi})^2}\right.$$

$$\left.+\frac{l}{24}\left[\frac{2l^2-3a^2}{(l^2+a^2)^{3/2}}-\frac{9\rho^2+2l^2}{(l^2+\rho^2)^{3/2}}\right]\frac{e^{i\chi}}{e^{\mp\xi}-e^{i\chi}}\right\}, \tag{82}$$

$$v_z \approx \frac{2d}{al^2}\frac{(l^2+a^2)^{3/4}}{\sqrt[4]{l^2+\rho^2}}\,\mathrm{Re}\left\{\frac{e^{\mp\xi+i\chi}}{(e^{\mp\xi}-e^{i\chi})^2}\pm\frac{l}{24}\left[\frac{3\rho^2-2l^2}{(l^2+\rho^2)^{3/2}}\right.\right.$$

$$\left.\left.-\frac{3a^2-2l^2}{(l^2+a^2)^{3/2}}\right]\frac{e^{i\chi}}{e^{\mp\xi}-e^{i\chi}}\right\}. \tag{83}$$

In Fig. 4, a comparison is made between the velocity fields of the monopole and the dipole inductions, for the same values of dimensionless helical pitch (h=1, 2, and 8). The thick lines show the axial and azimuthal velocity profiles for the monopole helical filament and the thin lines indicate the ones for the dipole filament with the strength $d/(\Gamma a)=-0.05$. The velocity is normalized by $\Gamma/(2\pi a)$. The structure of the dipole field as a sort of derivative of the monopole field is clearly seen. In contrast to the flow of the monopole origin which is accompanied by bulk axial motion inside the supporting cylinder, the dipole filament induces an intense fluid motion along the supporting cylinder. Except for a region close to the core, the influence of the dipoles is slight. At a small pitch, the velocity of the dipoles competes with that of the monopoles in the neighborhood of $x/a=-1$ as well. The helical dipole filaments of small pitch cause, around $x/a=-1$, an intensive jet-like flow in both the axial and the azimuthal directions with the maximum values attained on a cylinder close to the supporting cylinder.
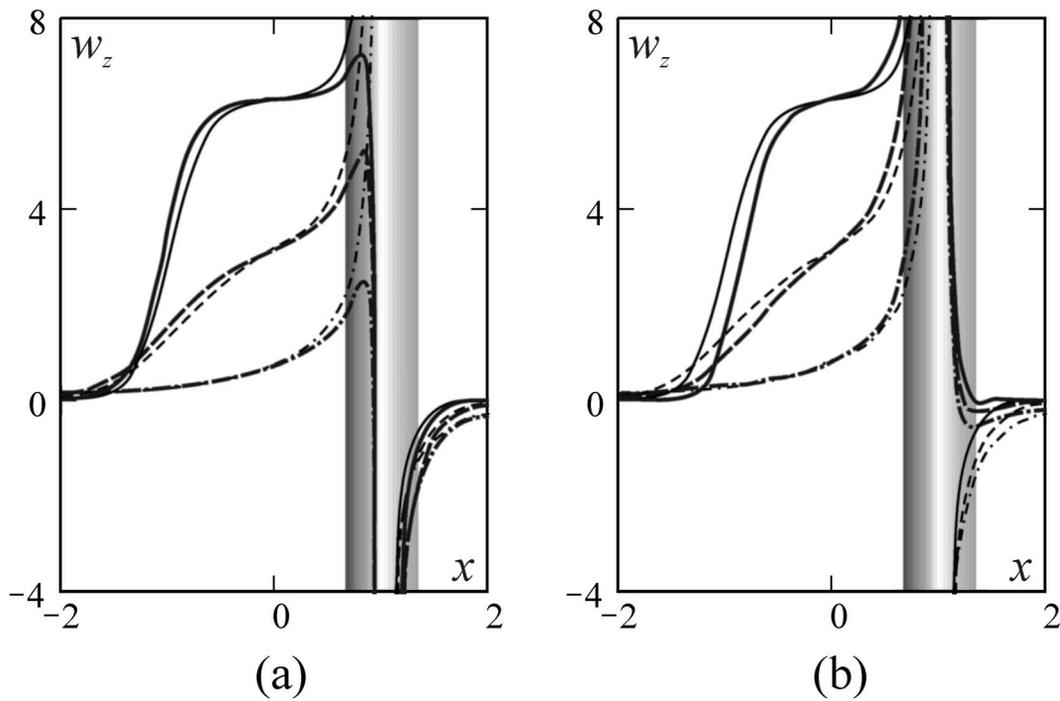
FIG. 5. Influence of dipoles on the axial velocity profiles along the Ox axis, at $z=0$, for different types of vorticity distribution in the core: (a) uniform core (36) and (b) Gaussian core (39). We pick out a few values of the helical pitch normalized by a: $h=1$ (solid lines), $h=2$ (dashed lines), and $h=8$ (dash-dotted lines). The thick lines correspond to the superposition $w_z=u_z+v_z$ of velocities, normalized by $\Gamma/(2\pi a)$, due to the monopoles and the dipoles for a helical vortex of finite-core radius $\sigma/a=0.33$, which should be compared with thin lines for the normalized velocity $w_z=u_z$ around a helical monopole filament. The horizontal axis is x/a.

D. Influence of dipoles on monopole field

In order to gain an insight into the influence of the dipoles relative to the monopoles, we exploit the simplified expressions (66) and (67), and (82) and (83), augmented by (62) and (79), for velocity field induced by the mono- and

the dipole helical filaments. Velocity field, the superposition of both contributions, is displayed with thick lines in typical cross sections, at the height $z=0$, in Figs. 5–9 for a specific core size $\sigma/a=0.33$. For comparison, the velocity induced by the monopoles alone is included with thin lines. We examine
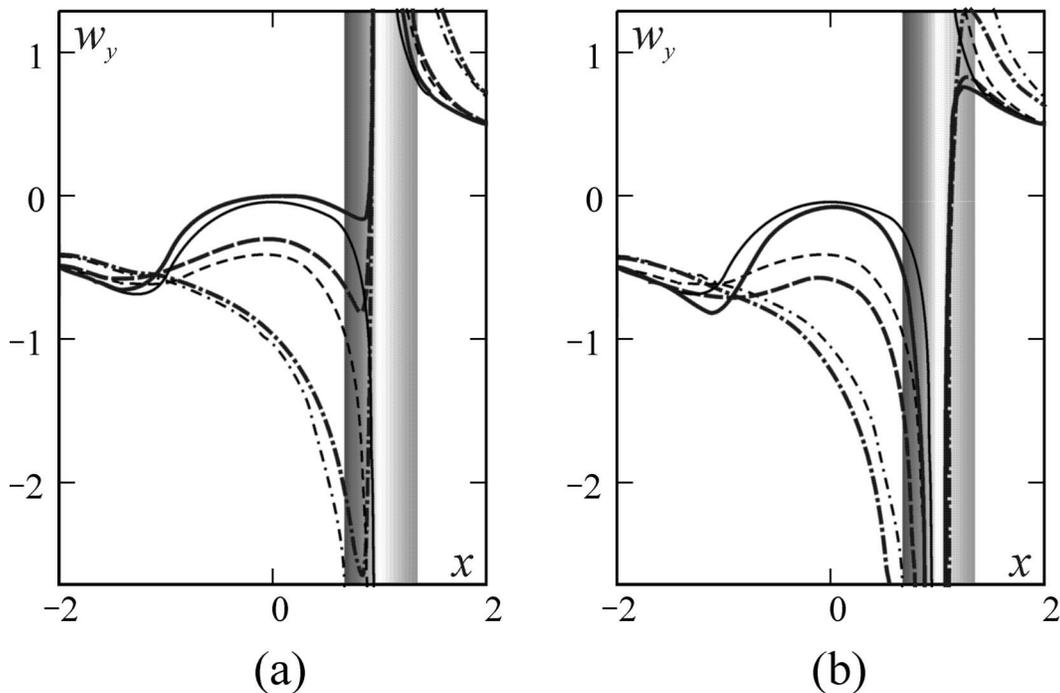

FIG. 6. As Fig. 5, but for the normalized azimuthal velocities $w_\phi=u_\phi+v_\phi$ (thick lines) and $w_\phi=u_\phi$ (thin lines); $w_y=-w_\phi$ for $x<0$ and $w_y=w_\phi$ for $x\geqslant 0$.
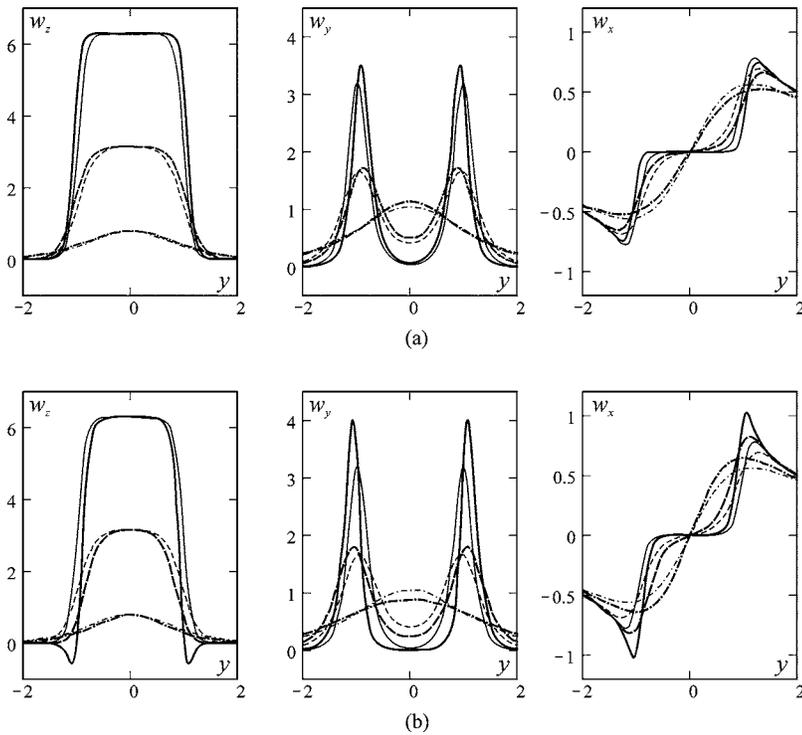
FIG. 7. Influence of dipoles on the axial (w_z), radial ($w_y = -w_\rho$ for $y < 0$ and $w_y = w_\rho$ for $y \geqslant 0$), and azimuthal ($w_x = -w_\phi$ for $y < 0$ and $w_x = w_\phi$ for $y \geqslant 0$) velocity profiles, normalized by $\Gamma/(2\pi a)$, along the Oy axis, at $z = 0$, for different types of vorticity distribution in the core: (a) uniform core (36) and (b) Gaussian core (39). We pick out a few values of the normalized helical pitch: $h = 1$ (solid lines), $h = 2$ (dashed lines), and $h = 8$ (dash-dotted lines). The thick lines correspond to the superposition of velocities due to the monopoles and the dipoles for a helical vortex of finite-core radius $\sigma/a = 0.33$, which should be compared with thin lines for the velocity around a helical monopole filament. The horizontal axis is y/a.

two typical vorticity profiles at $O(\epsilon^0)$, constant vorticity in the circular core (36), and the Gaussian distribution (39). The former is concerned with (a) and the latter with (b) of each figure. As representative values of helical pitch normalized by a, small, medium, and large, we again picked out $h = 1$ (solid lines), $h = 2$ (dashed lines), and 8 (dash-dotted lines).

Figures 5 and 6 draw velocity profiles on the plane including the symmetric (Oz) axis and the Ox axis, while Fig. 7 on the plane including the symmetric axis but the Oy axis. The vertical column marked with dark color is the region of thickness 0.66 centered on the supporting cylinder. This region is occupied by the vortical core of radius $\sigma/a = 0.33$, in which the velocity field produced in Secs. III and IV ceases to be valid. Figure 8 draws the variation of velocities with ϕ along the circle, at $z = 0$, on the cylindrical surface of $\rho/a = 0.67$ contained in the cylinder around which the tube
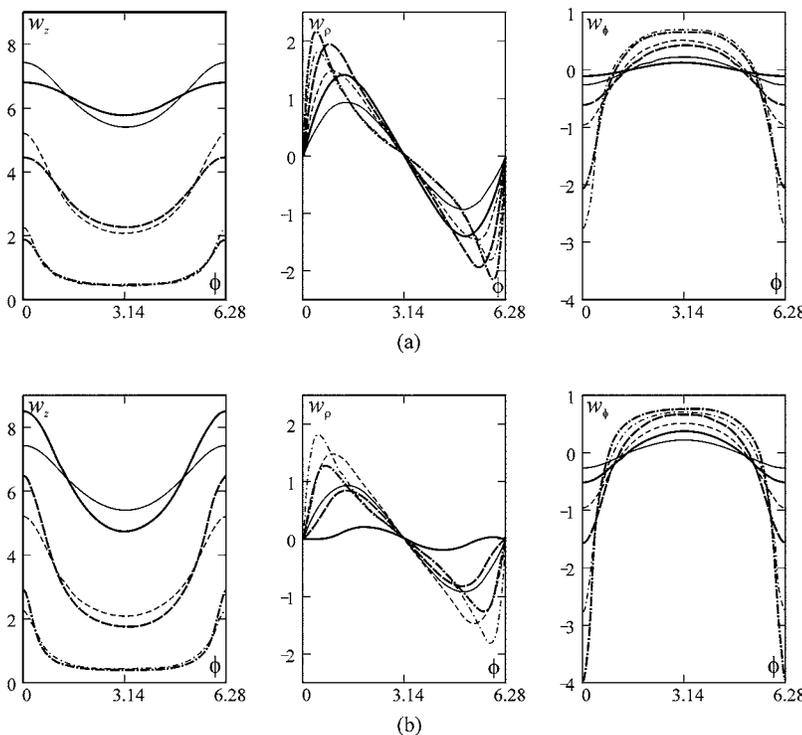

FIG. 8. Influence of dipoles on the axial (w_z), radial (w_ρ), and azimuthal (w_ϕ) velocity profiles, normalized by $\Gamma/(2\pi a)$, along the circle of $\rho/a = 0.67$, at $z = 0$, for different types of vorticity distribution in the core: (a) uniform core (36) and (b) Gaussian core (39). We pick out a few values of the normalized helical pitch: $h = 1$ (solid lines), $h = 2$ (dashed lines), and $h = 8$ (dash-dotted lines). The thick lines correspond to the superposition of velocities due to the monopoles and the dipoles for a helical vortex of finite-core radius $\sigma/a = 0.33$, which should be compared with thin lines for the velocity around a helical monopole filament.
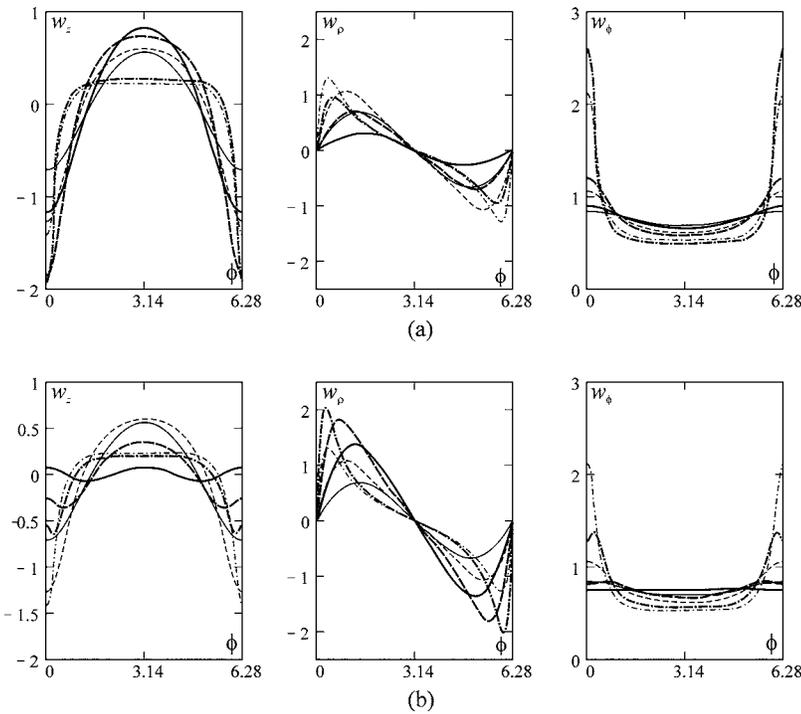
FIG. 9. As Fig. 8, but along the circle of $\rho/a=1.33$ outside the supporting cylinder.

centerline is wound, and Fig. 9 draws that along the intersecting circle of $z=0$ and the exterior cylinder of $\rho/a=1.33$. Both of the cylinders meet the core at $\phi=0$ and 2π.

The influence of the dipoles becomes significant in the neighborhood of the supporting cylinder, while it is immaterial around the central axis of the cylinder. The higher singularity of the dipole as represented by (76), compared with the monopole singularity (59), near the core is responsible for this behavior. The dipole influence is accentuated, for a given a, as the pitch $2\pi l$ is decreased and the core radius σ

is increased. The action of the dipoles on the axial and azimuthal velocities is complementary to the radial velocity; in a region where the dipole influence is large on the axial and azimuthal velocities it is small on the radial velocity, and vice versa. As is seen from Figs. 8 and 9, for the axial and azimuthal velocities, the dipole effect is large not only in the neighborhood of the core itself ($\phi=0$) but also near $\phi=\pi$, and, for the radial velocity, at angles in the midway between $\phi=0$ and $\phi=\pi$ and between $\phi=\pi$ and $\phi=2\pi$.
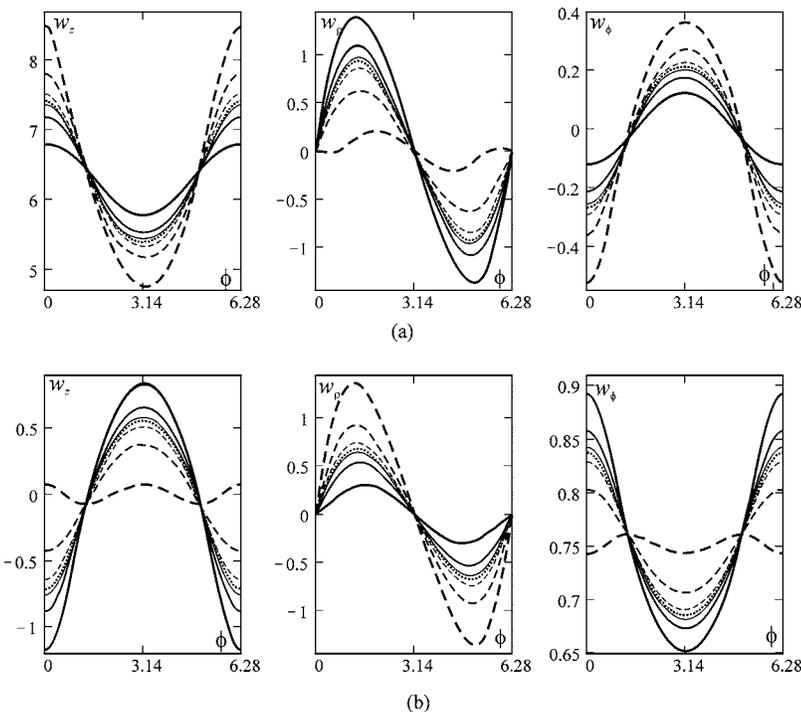
In Fig. 10, we inquire into the variation of the dipole

FIG. 10. Sensitivity, to the core size, of the influence of dipoles on the axial (w_z), radial (w_ρ), and azimuthal (w_ϕ) velocity profiles, normalized by $\Gamma/(2\pi a)$, along the circles of (a) $\rho/a=0.67$ inside the core and (b) $\rho/a=1.33$ outside the core, at $z=0$. The helical pitch is fixed to be $h=1$, but both the uniform core (36) (solid lines) and the Gaussian core (39) (dashed lines) are taken up. The thick lines correspond to $\sigma/a=0.33$, moderately thick lines to $\sigma/a=0.2$, and thin lines to $\sigma/a=0.1$. The case of infinitely thin core, or the monopole filament, is included with a dotted line.

influence with the core thickness σ. This is exemplified by the normalized velocity field, on the circle, at $z=0$, of radii $\rho/a=0.67$ (a) and $\rho/a=1.33$ (b), induced by a helical vortex of dimensionless pitch $h=1$ with values of $\sigma/a=0.1$, 0.2 and 0.33, a thicker line for a thicker core. The solid lines correspond to the uniform core, and the dashed lines to the Gaussian core. The velocity field around a thick core is affected, to a large extent, by the dipoles, implying that the approximation by the monopoles only is by no means justified.

V. CONCLUSION

Elongated vortices observed in practical situations are not necessarily slender. We have provided a systematic method for the asymptotic expansions of the Biot-Savart law that takes account of the finite thickness of vortex tube. We have demonstrated the advantage of Dyson's method as generalized to three dimensions. When combined with the method of matched asymptotic expansions, this technique saves a great deal of computations and moreover it manifests the dipole structure, in conjunction with curvature effect. This technique has a potential extensibility. A next-order correction from the quadrupoles, stemming from elliptical deformation of the core, will be incorporated without difficulty.

A helical vortex tube is amenable to a thorough analysis of the asymptotic formula. Hardin's solution[1] for the monopoles has been extended to include the dipoles. The resulting formulas for the vector potential and the velocity field have been worked out in the series form of Kapteyn's type. By summing up the major part of each term, we have successfully extracted the singular parts. It is noteworthy that this procedure remedies the divergence of the series occurring on the cylinder around which the central helical curve is wound. The velocity field induced by the dipoles is small near the axis of the supporting cylinder, but becomes larger as the cylinder is approached. For a small pitch and for a fat core, the correction from the dipoles could be comparable with and overturn the monopole field.

There are a diversity of applications, some of which were enumerated in the Introduction. The breakdown of vortices into helical structures[13,29–31] will call for the knowledge of the velocity field around thick helical vortices. For vortex rings, the accuracy of the asymptotic expansions of the Biot-Savart law near the core is better than expected, since the magnitude of the coefficients decreases exponentially with the order of the expansions.[16,19,32] It was concluded that expansions to $O(\epsilon^2)$ is sufficient for the velocity field around the ring and that expansions to $O(\epsilon^3)$ is sufficient for the traveling speed. This situation will be likely to carry over to three dimensions.

Recently a new instability mechanism caused by curvature effect of the tube centerline is proposed for vortex rings.[33,34] Presumably, the same instability mechanism is shared by a helical vortex tube. Torsion of the centerline may bring in yet unknown alterations. One of the limitations of the present treatment is the assumption of uniformity of the strength of the dipole $d^{(1)}$ along the vortex tube. This assumption rules out the local stretching of the core[35] and core-area waves that may play a vital role for disruption of vortical structures.[31,36,37] A systematic treatment of these effects remains as longstanding problems.

ACKNOWLEDGMENTS

APPENDIX A: EQUATIONS OF MOTION

This appendix collects the equations of motion to be solved for the inner solution in Appendix B.[25,26] We make dimensionless the coordinates $\mathbf{x}$ defined by (1), the time t, the velocity field $\mathbf{u}$ defined by (3), and the pressure p with use of σ_0 and R_0, being the measures of the core radius and the curvature radius, respectively. Attached with a star, they are expressed as

$$\left.\begin{array}{l} r = \sigma_0 r^*, \quad \xi = R_0 \xi^*, \quad X = R_0 X^*, \quad \kappa = \dfrac{\kappa^*}{R_0}, \quad \tau = \dfrac{\tau^*}{R_0}, \quad t = \dfrac{R_0^2}{\Gamma} t^* \\[2mm] (u,v,w) = \dfrac{\Gamma}{\sigma_0}(u^*,v^*,w^*), \quad \psi = \Gamma \psi^*, \quad \dot{X} = \dfrac{\Gamma}{R_0} \dot{X}^*, \quad \dfrac{p}{\rho_f} = \left(\dfrac{\Gamma}{\sigma_0}\right)^2 p^* \end{array}\right\}, \tag{A1}$$

where ρ_f is the fluid density. The symbol over dot designates partial differentiation with respect to t, holding r, θ, and ξ fixed. We write down the dimensionless form of the Navier-Stokes equations and their curl, viewed from the local moving coordinates (r, θ, ξ), along with the subsidiary relation

that holds between ζ and ψ, the axial vorticity (6) and the streamfunction (24).

Dropping the stars, the Navier-Stokes equations for the variables (3), expressed in terms of the moving coordinates (r, θ, ξ) introduced in Sec. II A, takes the following form:

$$\epsilon^3 \ddot{X} \cdot e_r + \epsilon^2 \left[\dot{u} + w(\dot{t} \cdot e_r) - (\dot{e}_r \cdot e_\theta) \frac{\partial u}{\partial \theta} \right]$$

$$+ \frac{\epsilon}{h_3} [w + \epsilon^2 r(\dot{t} \cdot e_r)] \left(\epsilon \frac{\partial \dot{X}}{\partial \xi} \cdot e_r + \frac{\partial u}{\partial \xi} + \eta \kappa w \cos \varphi \right)$$

$$+ u \frac{\partial u}{\partial r} + \frac{v}{r} \left(\frac{\partial u}{\partial \theta} - v \right) = - \frac{\partial p}{\partial r} + [\text{viscous term}], \quad (A2)$$

$$\epsilon^3 \ddot{X} \cdot e_\theta + \epsilon^2 \left[\dot{v} + w(\dot{t} \cdot e_\theta) - (\dot{e}_r \cdot e_\theta) \frac{\partial v}{\partial \theta} \right]$$

$$+ \frac{\epsilon}{h_3} [w + \epsilon^2 r(\dot{t} \cdot e_r)] \left(\epsilon \frac{\partial \dot{X}}{\partial \xi} \cdot e_\theta + \frac{\partial v}{\partial \xi} - \eta \kappa w \sin \varphi \right)$$

$$+ u \frac{\partial v}{\partial r} + \frac{v}{r} \left(\frac{\partial v}{\partial \theta} + u \right) = - \frac{1}{r} \frac{\partial p}{\partial \theta} + [\text{viscous term}],$$

$$(A3)$$

$$\epsilon^3 \ddot{X} \cdot t + \epsilon^2 \left[\dot{w} - u(\dot{t} \cdot e_r) - v(\dot{t} \cdot e_\theta) - (\dot{e}_r \cdot e_\theta) \frac{\partial w}{\partial \theta} \right]$$

$$+ \frac{\epsilon}{h_3} [w + \epsilon^2 r(\dot{t} \cdot e_r)] \left[\epsilon \frac{\partial \dot{X}}{\partial \xi} \cdot t + \frac{\partial w}{\partial \xi} - \eta \kappa (u \cos \varphi \right.$$

$$\left. - v \sin \varphi) \right] + \left(u \frac{\partial}{\partial r} + \frac{v}{r} \frac{\partial}{\partial \theta} \right) w$$

$$= - \frac{\epsilon}{h_3} \frac{\partial p}{\partial \xi} + [\text{viscous term}]. \quad (A4)$$

Here h_3 is defined by (7), whose dimensionless form is $h_3 = \eta(1 - \epsilon \kappa r \cos \varphi)$. The viscous term is written in a vectorial form as[25]

$$[\text{viscous term}] = \frac{\epsilon^2 \nu}{\Gamma} \frac{1}{h_3} \frac{\partial}{\partial \xi} \left(\frac{1}{h_3} \frac{\partial \dot{X}}{\partial \xi} \right)$$

$$+ \frac{\nu}{\Gamma} \nabla^2 (u e_r + v e_\theta + w t), \quad (A5)$$

where ν is the kinematic viscosity. Elimination of the pressure p from (A2) and (A3) by trial and error is not easy, and this procedure is facilitated by turning to the vorticity equations, the curl of the Navier-Stokes equations. The vorticity equation in the axial direction is deduced to be

$$\epsilon^2 [\dot{\zeta} - (\dot{t} \cdot e_r) \omega_r - (\dot{t} \cdot e_\theta) \omega_\theta] + \frac{\epsilon}{h_3} [w + \epsilon^2 r(\dot{t} \cdot e_r)]$$

$$\times \left[\frac{\partial \zeta}{\partial \xi} - \eta \kappa (\omega_r \cos \varphi - \omega_\theta \sin \varphi) \right]$$

$$- \epsilon^2 (\dot{e}_r \cdot e_\theta) \frac{\partial \zeta}{\partial \theta} + u \frac{\partial \zeta}{\partial r} + \frac{v}{r} \frac{\partial \zeta}{\partial \theta}$$

$$= \omega_r \frac{\partial w}{\partial r} + \frac{\omega_\theta}{r} \frac{\partial w}{\partial \theta} + \epsilon \frac{\zeta}{h_3} \frac{\partial w}{\partial \xi} - \frac{\epsilon \eta}{h_3} \kappa (u \cos \varphi - v \sin \varphi) \zeta$$

$$+ \frac{\epsilon^2}{h_3} \left(\frac{\partial \dot{X}}{\partial \xi} \cdot t \right) \zeta + [\text{viscous term}]. \quad (A6)$$

The use of the vector potential A enables us to skip the equation of continuity. The vector potential or the stream-function ψ, introduced as (24) in Sec. II C, is tied with the relative velocity (u,v) in the transversal plane via

$$u = \frac{\eta}{h_3 r} \frac{\partial \psi}{\partial \theta} - \frac{\epsilon}{h_3} \frac{\partial A_\theta}{\partial \xi} - \epsilon[(\dot{X} \cdot n)\cos \varphi + (\dot{X} \cdot b)\sin \varphi],$$

$$(A7)$$

$$v = - \frac{\eta}{h_3} \frac{\partial \psi}{\partial r} + \frac{\epsilon}{h_3} \frac{\partial A_r}{\partial \xi} + \epsilon[(\dot{X} \cdot n)\sin \varphi - (\dot{X} \cdot b)\cos \varphi].$$

$$(A8)$$

Introducing these into (6) produces the subsidiary condition relating ψ to the axial vorticity ζ, which is written to $O(\epsilon)$ as

$$\frac{1}{r} \frac{\partial}{\partial r} \left(r \frac{\partial \psi}{\partial r} \right) + \frac{1}{r^2} \frac{\partial^2 \psi}{\partial \theta^2} + \frac{\epsilon \eta}{h_3} \kappa \left(\cos \varphi \frac{\partial \psi}{\partial r} - \frac{\sin \varphi}{r} \frac{\partial \psi}{\partial \theta} \right)$$

$$+ O(\epsilon^2) = - \frac{h_3}{\eta} \zeta. \quad (A9)$$

Here use has been made of the Coulomb-gauge condition (9). Alternatively this is obtainable directly from $\nabla^2 A = -\boldsymbol{\omega}$.

APPENDIX B: INNER SOLUTION

We are concerned with a *quasisteady* motion of a vortex tube with vorticity profile uniform along it. In the presence of viscosity, the core radius grows with time as $\sigma \sim (\nu t)^{1/2}$. The time scale characterizing the quasisteady motion of the segment of curvature radius R_0 is $t \sim R_0^2/\Gamma$, the time taken for the vortex filament with local speed $\sim \Gamma/R_0$ to traverses a few curvature radii. The ratio of core radius to curvature radius is $\epsilon = \sigma/R_0 \sim (\nu/\Gamma)^{1/2}$, and consequently the viscous term (A5) is considered to be of $O(\epsilon^2)$.[17,19,25]

In our setting, the leading-order flow field consists only of circulatory motion with both rotational and translational symmetries about the local central axis, and we pose the following form for the perturbation solution in a power series in ϵ:

$$u = \epsilon u^{(1)} + \cdots, \quad v = v^{(0)}(r,t) + \epsilon v^{(1)} + \cdots,$$

$$w = \epsilon w^{(1)} + \epsilon^2 w^{(2)} + \cdots, \quad \dot{X} = \dot{X}^{(0)} + \cdots. \quad (B1)$$

The axial velocity $w^{(1)}$, of $O(\epsilon)$, is supposed to be independent of r and θ as will be stated below. According to our normalization (A1), $\dot{X}^{(0)}$ is looked upon as first order. Stretching of vortex lines may enter through dependence on t of $v^{(0)}$. Correspondingly, the streamfunction ψ is expanded as

$$\psi = \psi^{(0)}(r,t) + \epsilon \psi^{(1)} + \cdots, \quad (B2)$$

the leading-order term of which gives

$$v^{(0)} = - \frac{\partial \psi^{(0)}}{\partial r}. \quad (B3)$$

In the absence of viscosity, the functional form of $v^{(0)}(r)$ may be arbitrary. The viscosity selects the profile, in favor of a Gaussian distribution of vorticity, but at $O(\epsilon^2)$.[19]

A glimpse of (4)–(6), substituted from (B1), tells us that

$$\omega_r = \epsilon^2 \omega_r^{(2)} + \cdots, \qquad \omega_\theta = \epsilon^2 \omega_\theta^{(2)} + \cdots,$$

$$\zeta = \zeta^{(0)}(r) + \epsilon \zeta^{(1)} + \cdots, \qquad (B4)$$

with

$$\zeta^{(0)} = \frac{1}{r}\frac{d}{dr}[rv^{(0)}]. \qquad (B5)$$

In conformity with our intention as dictated in Sec. II B, the vorticity is dominated by the tangential component. The Euler equations are immediately integrated for the pressure of $O(\epsilon^0)$ as

$$p^{(0)} = \int_0^r \frac{[v^{(0)}(r')]^2}{r'} dr'. \qquad (B6)$$

At first order, the necessary terms among (A6) are merely

$$u^{(1)}\frac{\partial \zeta^{(0)}}{\partial r} + \frac{v^{(0)}}{r}\frac{\partial \zeta^{(1)}}{\partial \theta} = \kappa v^{(0)} \zeta^{(0)} \sin \varphi, \qquad (B7)$$

which is to be integrated for $\zeta^{(1)}$. The filament speed $\dot{X}^{(0)}$ is determined by the matching condition of the inner solution to the outer one,[25,26,38] but we may leave the detailed form of $\dot{X}^{(0)}$ unspecified for our purpose. When the vector potential A in its inner limit is expanded in powers of ϵ, the transversal components $(A_r^{(0)}, A_\theta^{(0)})$ of $O(\epsilon^0)$ are of nonlocal origin and are functions of ξ and t only. The Coulomb-gauge condition (9) becomes

$$A_r^{(0)} + \frac{\partial A_\theta^{(0)}}{\partial \theta} = 0. \qquad (B8)$$

A simplification of the expression of the first-order velocity is achieved by posing

$$\psi^{(1)} = [\kappa \hat{\psi}_{11}^{(1)} + r B_{11}^{(1)}]\cos \varphi + [\kappa \hat{\psi}_{12}^{(1)} + r B_{12}^{(1)}]\sin \varphi, \qquad (B9)$$

and choosing $B_{11}^{(1)}$ and $B_{12}^{(1)}$, functions of ξ and t, as

$$B_{11}^{(1)} = \frac{1}{\eta}\frac{\partial A_{r1}^{(0)}}{\partial \xi} - \tau A_{r2}^{(0)} - \dot{X}^{(0)} \cdot \boldsymbol{b},$$

$$B_{12}^{(1)} = \frac{1}{\eta}\frac{\partial A_{r2}^{(0)}}{\partial \xi} + \tau A_{r1}^{(0)} + \dot{X}^{(0)} \cdot \boldsymbol{n}, \qquad (B10)$$

where the decomposition $A_r^{(0)} = A_{r1}^{(0)} \cos \varphi + A_{r2}^{(0)} \sin \varphi$ should be understood. The terms of nonlocal origin are all absorbed into $B_{11}^{(1)}$ and $B_{12}^{(1)}$, and the first-order terms of (A7) and (A8) comprise local functions only:

$$u^{(1)} = -\frac{\kappa}{r}[\hat{\psi}_{11}^{(1)} \sin \varphi - \hat{\psi}_{12}^{(1)} \cos \varphi], \qquad (B11)$$

$$v^{(1)} = -\kappa\left\{\left[\frac{\partial \hat{\psi}_{11}^{(1)}}{\partial r} - rv^{(0)}\right]\cos \varphi + \frac{\partial \hat{\psi}_{12}^{(1)}}{\partial r}\sin \varphi\right\}. \qquad (B12)$$

With (B11) for $u^{(1)}$, (B7) is readily integrated with respect to θ to yield

$$\zeta^{(1)} = \kappa[\hat{\zeta}_{11}^{(1)} \cos \varphi + \hat{\zeta}_{12}^{(1)} \sin \varphi] + \zeta_0^{(1)}(r), \qquad (B13)$$

where

$$\hat{\zeta}_{11}^{(1)} = -[\alpha \hat{\psi}_{11}^{(1)} + r\zeta^{(0)}], \quad \hat{\zeta}_{12}^{(1)} = -\alpha \hat{\psi}_{12}^{(1)}, \qquad (B14)$$

and α is defined by (26). We ignore the arbitrary axisymmetric function $\zeta_0^{(1)}$ as this may be absorbed into the arbitrary function $\zeta^{(0)}$ in the inviscid case.

When coupled with (B13), the subsidiary relation (A9) leads, up to $O(\epsilon)$, to

$$\left[\frac{\partial^2}{\partial r^2} + \frac{1}{r}\frac{\partial}{\partial r} - \left(\frac{1}{r^2} + \alpha\right)\right]\hat{\psi}_{11}^{(1)} = v^{(0)} + 2r\zeta^{(0)}, \qquad (B15)$$

$$\left[\frac{\partial^2}{\partial r^2} + \frac{1}{r}\frac{\partial}{\partial r} - \left(\frac{1}{r^2} + \alpha\right)\right]\hat{\psi}_{12}^{(1)} = 0. \qquad (B16)$$

A solution finite at $r=0$ is[25]

$$\hat{\psi}_{11}^{(1)} = \Psi_{11}^{(1)} + c_{11}^{(1)} v^{(0)}, \quad \hat{\psi}_{12}^{(1)} = c_{12}^{(1)} v^{(0)}, \qquad (B17)$$

with

$$\Psi_{11}^{(1)} = v^{(0)}\left\{\frac{r^2}{2} + \int_0^r \frac{dr'}{r'[v^{(0)}(r')]^2}\int_0^{r'} r''[v^{(0)}(r'')]^2 dr''\right\}, \qquad (B18)$$

and $c_{11}^{(1)}$ and $c_{12}^{(1)}$ are constants bearing with the freedoms of shifting the local origin $r=0$ of the moving frame, in the $\boldsymbol{n}$ and $\boldsymbol{b}$ directions, respectively, within an accuracy of $O(\epsilon^2)$.[16,19] The core shape is symmetric with respect to a particular line parallel to local $\boldsymbol{n}$ vector. A judicious choice of the origin should be some point on this line. This choice demands that $c_{12}^{(1)} = 0$ or

$$\hat{\psi}_{12}^{(1)} \equiv 0. \qquad (B19)$$

Noting that $v^{(0)} \sim 1/(2\pi)$ as $r \to \infty$, the first of (B17) behaves at large distances $(1 \ll r \ll 1/\epsilon)$ as

$$\hat{\psi}_{11}^{(1)} \sim \frac{1}{4\pi}\left(\log r + A + \frac{1}{2}\right)r + \frac{d^{(1)}}{r}, \qquad (B20)$$

where

$$A = \lim_{r \to \infty}\left\{4\pi^2 \int_0^r r'[v^{(0)}(r')]^2 dr' - \log r\right\}. \qquad (B21)$$

By evaluating (34) at small values of r, the inner limit of the outer solution, the strength $d^{(1)}$ of dipole is shown to agree with (23) in parallel with the axisymmetric problem.[19] As is evident from (B17), $d^{(1)}$ depends on the choice of $c_{11}^{(1)}$ and therefore of location of the origin $r=0$. The lowest-order terms of the axial component (A4) of the Navier-Stokes equations, which are of $O(\epsilon)$, consist of

$$\frac{v^{(0)}}{r}\frac{\partial w^{(1)}}{\partial \theta} = 0. \qquad (B22)$$

The axisymmetric solution $w^{(1)} = w^{(1)}(\xi, t)$ could be the local uniform axial velocity, independent of r and θ, induced by the rest of the filament, which meets the matching condition.

We are now ready to make headway to second order. The pressure $p^{(1)}$ of $O(\epsilon)$ is obtained from the transversal components of the Navier-Stokes equations (A2) and (A3):

$$\frac{\partial p^{(1)}}{\partial r} = -\frac{v^{(0)}}{r}\left[\frac{\partial u^{(1)}}{\partial \theta} - 2v^{(1)}\right],$$

$$\frac{1}{r}\frac{\partial p^{(1)}}{\partial \theta} = -u^{(1)}\frac{\partial v^{(0)}}{\partial r} - \frac{v^{(0)}}{r}\left[\frac{\partial v^{(1)}}{\partial \theta} + u^{(1)}\right]. \tag{B23}$$

Thanks to (B11) and (B12), an explicit form of $p^{(1)}$ is brought in from simultaneous integration of (B23) as

$$p^{(1)} = \kappa\left(v^{(0)}\frac{\partial \hat{\psi}_{11}^{(1)}}{\partial r} - \zeta^{(0)}\hat{\psi}_{11}^{(1)} - r[v^{(0)}]^2\right)\cos\varphi. \tag{B24}$$

The gradient of $p^{(1)}$, in turn, drives axial flow at $O(\epsilon^2)$. Collecting $O(\epsilon^2)$ terms in (A4), we are left with

$$-v^{(0)}[\boldsymbol{e}_\theta\cdot\boldsymbol{i}^{(0)}] + \kappa v^{(0)}w^{(1)}\sin\varphi + \frac{v^{(0)}}{r}\frac{\partial w^{(2)}}{\partial \theta} = -\frac{1}{\eta}\frac{\partial p^{(1)}}{\partial \xi}. \tag{B25}$$

The viscous term is of higher order. Equation (B25) admits a compact form of the solution for $w^{(2)}$ as

$$w^{(2)} = r\left[\frac{\partial \hat{\psi}_{11}^{(1)}}{\partial r} - \frac{\zeta^{(0)}}{v^{(0)}}\hat{\psi}_{11}^{(1)} - rv^{(0)}\right](\kappa\tau\cos\varphi - \kappa_s\sin\varphi)$$

$$+ \frac{r}{\eta}\frac{\partial \dot{\boldsymbol{X}}^{(0)}}{\partial \xi}\cdot\boldsymbol{e}_r + \kappa rw^{(1)}\cos\varphi + w_0^{(2)}. \tag{B26}$$

The detailed form of $w_0^{(2)}$ is unnecessary for obtaining a correction of the Biot-Savart law.

We are convinced from (B26) that torsion or arcwise variation of curvature is requisite for the presence of pressure gradient and thus for emergence of axial velocity at $O(\epsilon^2)$. This is a genuinely three-dimensional effect peculiar to curved vortex tubes, which is missing for circular rings.

APPENDIX C: THE EVALUATION OF THE KAPTEYN'S-TYPE SERIES

The series of Kapteyn's type (47) generalizes the well-known Kapteyn series[27] $\partial[\Sigma_{m=1}^{\infty}I_m(mb)K_m(ma)]/\partial b$ to fit into trigonometric series. Let the coefficient of the trigonometric series (47) be $hi_m(x,y,I,J,M)$, namely,

$$hi_m(x,y,I,J,M) = m^M I_m^{\langle I\rangle}(mx)K_m^{\langle J\rangle}(my), \tag{C1}$$

where the superscript $\langle I\rangle$ designates the Ith derivative with respect to the argument, with $I_m^{(0)}(mx)=I_m(mx)$, and similarly for $\langle J\rangle$. This series is convergent for $x<y$.

Figure 11(a) shows the behavior of coefficients $hi_m(x,1,0,1,1)$ of the trigonometric series (47). We recognize that the coefficients grow indefinitely with m in the neighborhood of $x=y(=1)$, invalidating the approach of using the series there.

With a view to sidestepping this difficulty, we introduce strained spatial variables and extract the dominant parts, in terms of elementary functions only, from the modified Bessel functions, and then perform their summation in (47). This
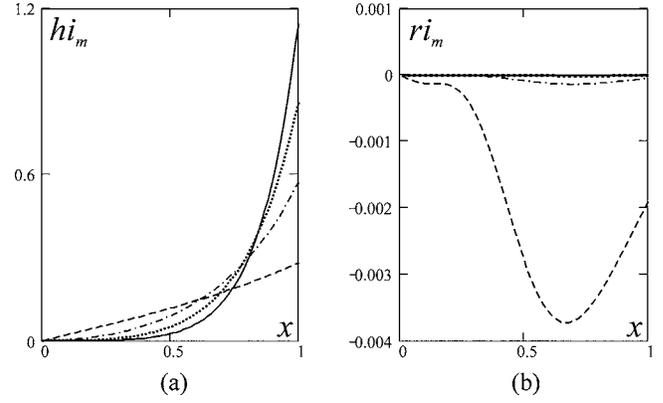

FIG. 11. Spatial variation of the coefficients of trigonometric series. (a) Kapteyn's type $hi_m(x,1,0,1,1)$ defined by (C1), and (b) the remainder $ri_m(x,1,0,1,1)$ of the series defined by (C13). $m=1$ (dashed lines), 2 (dash-dotted lines), 3 (dotted lines), and 4 (solid lines).

approach was previously employed for the monopole field, that is, for the case of $M,I,J=0$ and 1.[9] We extend this technique to $M=2$ so as to be applicable to a helical filament with dipole and higher-pole singularities.

First, we formally substitute, into (47), high-order (m) asymptotics of the modified Bessel functions [Eqs. (9.7.7)–(10) of Abramowitz and Stegun[39]]. Their summations to $m=\infty$ result in closed forms of the known elementary functions, the first few of which are

$$\frac{e^{\xi+i\chi}}{(e^\xi - e^{i\chi})^2} = \sum_{m=1}^{\infty} m\exp[-m(\xi - i\chi)],$$

$$\frac{e^{i\chi}}{e^\xi - e^{i\chi}} = \sum_{m=1}^{\infty}\exp[-m(\xi - i\chi)],$$

$$\log(1 - e^{-\xi+i\chi}) = \sum_{m=1}^{\infty}\frac{1}{m}\exp[-m(\xi - i\chi)], \tag{C2}$$

$$\mathrm{Li}_2(e^{-\xi+i\chi}) = \sum_{m=1}^{\infty}\frac{1}{m^2}\exp[-m(\xi - i\chi)],$$

$$\mathrm{Li}_3(e^{-\xi+i\chi}) = \sum_{m=1}^{\infty}\frac{1}{m^3}\exp[-m(\xi - i\chi)].$$

In this way, we arrive at a representation of principal part $S_M^{I,J}$ of the series (47) as

$$S_M^{I,J} = \lambda^{I,J}\left[b_{M,0}^{I,J}\frac{e^{-\xi+i\chi}}{(e^{-\xi} - e^{i\chi})^2} + b_{M,1}^{I,J}\frac{e^{i\chi}}{e^{-\xi} - e^{i\chi}} + b_{M,2}^{I,J}\log(1 \right.$$

$$\left. - e^{\xi+i\chi}) + b_{M,3}^{I,J}\mathrm{Li}_2(e^{\xi+i\chi}) + b_{M,4}^{I,J}\mathrm{Li}_3(e^{\xi+i\chi})\right], \tag{C3}$$

where Li_2 and Li_3 are the polylogarithms, similarly to (58),

$$e^{\xi(x,y)} = \frac{x}{y}\frac{(1+\sqrt{1+y^2})\exp(\sqrt{1+x^2})}{(1+\sqrt{1+x^2})\exp(\sqrt{1+y^2})}, \tag{C4}$$

TABLE I. Comparison of approximations, at different accuracy levels (pole; pole+logarithm; or pole +logarithm+polylogarithm), with the values calculated via the integral representation (C11) by Wood and Boersma (Ref. 28) for the Kapteyn series at different radial arguments x and fixed angle π.

x	Integral (C11)[a]	Pole	Difference (%)	Pole+ logarithm	Difference (%)	Pole+logarithm +polylogarithm	Difference (%)
100	−0.002 483	−0.0025	0	−0.002 483	0	−0.002 483	0
20	−0.012 068	−0.0125	0.04	−0.012 068	0	−0.012 068	0
10	−0.023 285	−0.025	0.17	−0.023 293	0	−0.023 285	0
5	−0.043 391	−0.05	0.66	−0.043 465	0.01	−0.043 387	0
2	−0.096 111	−0.125	2.89	−0.094 002	−0.21	−0.095 614	−0.05
1	−0.197 607	−0.25	5.24	−0.188 734	−0.89	−0.204 920	0.73
0.5	−0.435 385	−0.5	6.46	−0.438 003	0.26	−0.426 714	−0.87
0.33	−0.685 602	−0.75	6.44	−0.700 682	1.51	−0.669 290	−1.63
0.2	−1.191 887	−1.25	5.81	−1.217 323	2.54	−1.184 050	−0.78
0.1	−2.455 668	2.5	4.43	−2.482 928	2.73	−2.462 022	0.64

[a]Reference 28.

$$\lambda^{I,J}(x,y) = \frac{1}{2} \frac{(\sqrt{1+x^2})^{I-1/2}(\sqrt{1+y^2})^{J-1/2}}{x^I(-y)^J}, \qquad (C5)$$

and $b_{M,k}^{I,J}$ is the $(M+1)(k+1)$th entry of the matrix

$$b^{I,J} = \begin{bmatrix} 0 & 0 & 1 & \alpha^{I,J} & \beta^{I,J} \\ 0 & 1 & \alpha^{I,J} & \beta^{I,J} & \gamma^{I,J} \\ 1 & \alpha^{I,J} & \beta^{I,J} & \gamma^{I,J} & 0 \end{bmatrix}. \qquad (C6)$$

The coefficients in (C3), or the entries of (C6), are obtained as a result of multiplication of the uniform expansions of the modified Bessel functions.

$$\alpha^{I,J}(x,y) = (1-I)\vartheta_1(x) - (1-J)\vartheta_1(y) + Iv_1(x) - Jv_1(y), \qquad (C7)$$

$$\beta^{I,J}(x,y) = (1-I)\vartheta_2(x) + (1-J)\vartheta_2(y) + Iv_2(x)$$
$$+ Jv_2(y) - (1-I)(1-J)\vartheta_1(x)\vartheta_1(y)$$
$$- J(1-I)\vartheta_1(x)v_1(y) - I(1-J)\vartheta_1(y)v_1(x)$$
$$- IJv_1(x)v_1(y), \qquad (C8)$$

$$\gamma^{I,J}(x,y) = (1-I)\vartheta_3(x) - (1-J)\vartheta_3(y) + Iv_3(x) - Jv_3(y) + (1-I)(1-J)[\vartheta_1(x)\vartheta_2(y) - \vartheta_2(x)\vartheta_1(y)] + J(1-I)[\vartheta_1(x)v_2(y)$$
$$- \vartheta_2(x)v_1(y)] + I(1-J)[\vartheta_2(y)v_1(x) - \vartheta_1(y)v_2(x)] + IJ[v_1(x)v_2(y) - v_2(x)v_1(y)], \qquad (C9)$$

where, using $t = (1+x^2)^{-1/2}$,

$$\vartheta_1 = (3t - 5t^3)/24, \quad v_1 = (-9t + 7t^3)/24,$$

$$\vartheta_2 = (81t^2 - 462t^4 + 385t^6)/1152,$$

$$v_2 = (-135t^2 + 594t^4 - 455t^6)/1152,$$

$$\vartheta_3 = (303\ 75t^3 - 369\ 603t^5 + 765\ 765t^7$$
$$- 425\ 425t^9)/414\ 720,$$

$$v_3 = (-425\ 25t^3 + 451\ 737t^5 - 883\ 575t^7$$
$$+ 475\ 475t^9)/414\ 720. \qquad (C10)$$

In Table I, our approximation $S_M^{I,J}$ to (47) is compared with the data taken from Table I of Wood and Boersma.[28] According to their definition of W, the series (47) with $(I,J)=(0,1)$ is represented, at $x=y$, as

$$\sum_{m=1}^{\infty} mI_m(mx)K_m'(mx)e^{im\chi}$$
$$= \frac{1}{2x} - \frac{1}{4x^2} \int_0^{\infty} \frac{\sin^2(t-\chi/2)}{[t^2/x^2 + \sin^2(t-\chi/2)]^{3/2}}dt, \qquad (C11)$$

where $0 < \chi < 2\pi$.

The integral (C11) cannot be implemented in a closed form, but was calculated numerically with six significant digits for many values of $1/x$,[28] and serves as a test for (C3). In Table I, we list the values of (C3), at $\chi = \pi$, for a choice of typical values of x, varying the accuracy levels (pole, pole +logarithm and pole+logarithm+polylogarithm). These values are assessed by the values of integral form (C11). We realize that, in the whole range of x examined, the maximal error does not exceed 6.5% even in the crudest approximation by the pole alone, and the error is diminished to 2.7% and 1.63% by correcting with logarithm and polylogarithms, respectively. For practical purposes, the handy approxima-

tion by the first two or three terms seems to be tolerable.

A further improvement in approximation is feasible by correcting with a few remaining nonsingular terms.

$$R_M^{I,J} = H_M^{I,J}(x,y,\chi) - S_M^{I,J}(x,y,\chi) = \sum_{m=1}^{\infty} ri_m(x,y,I,J,M)e^{im\chi},$$

$$(C12)$$

where

$$ri_m(x,y,I,J,M) = m^M I_m^{\langle I \rangle}(mx) K_m^{\langle J \rangle}(my) - m^{M-1} \lambda^{I,J} e^{m\xi(x,y)}$$

$$\times \left(1 + \frac{\alpha^{I,J}}{m} + \frac{\beta^{I,J}}{m^2} + \frac{\gamma^{I,J}}{m^3}\right). \quad (C13)$$

Figure 11(b) shows the behavior of coefficients $ri_m(x,1,0,1,1)$. In contrast to the series (47), the decrease in magnitude of the coefficients with m is rapid in the whole range of x. In the event that a high accuracy is required, we may augment our expansion with a finite truncation of (C12).

[1]J. C. Hardin, "The velocity field induced by a helical vortex filament," Phys. Fluids **25**, 1949 (1982).

[2]N. E. Joukowski, "Vortex theory of a rowing helical," Trudy Otdeleniya Fizicheskikh Nauk Imperatorskogo Obshchestva Lyubitelei Estestvoznaniya **16**, 1 (1912).

[3]H. Levy and A. G. Forsdyke, "The steady motion and stability of a helical vortex," Proc. R. Soc. London, Ser. A **120**, 670 (1928).

[4]S. E. Widnall, "The stability of a helical vortex filament," J. Fluid Mech. **54**, 641 (1972).

[5]D. W. Moore and P. G. Saffman, "The motion of a vortex filament with axial flow," Philos. Trans. R. Soc. London, Ser. A **272**, 403 (1972).

[6]R. L. Ricca, "The effect of torsion on the motion of a helical vortex filament," J. Fluid Mech. **273**, 241 (1994).

[7]P. A. Kuibin and V. L. Okulov, "Self-induced motion and asymptotic expansion of the velocity field in the vicinity of a helical vortex filament," Phys. Fluids **10**, 607 (1998).

[8]J. Boersma and D. H. Wood, "On the self-induced motion of a helical vortex," J. Fluid Mech. **384**, 263 (1999).

[9]V. L. Okulov, "The velocity field induced by vortex filaments with cylindrical and conic supporting surface," Russ. J. Eng. Thermophys. **5**, 63 (1995).

[10]A. Adebiyi, "On the existence of steady helical vortex tubes of small cross-section," Q. J. Mech. Appl. Math. **34**, 153 (1981).

[11]M. J. Landman, "On the generation of helical waves in circular pipe flow," Phys. Fluids A **2**, 738 (1990).

[12]D. G. Dritschel, "Generalized helical Beltrami flows in hydrodynamics and magnetohydrodynamics," J. Fluid Mech. **222**, 525 (1991).

[13]S. V. Alekseenko, P. A. Kuibin, V. L. Okulov, and S. I. Shtork, "Helical vortices in swirl flow," J. Fluid Mech. **382**, 195 (1999).

[14]S. C. Crow, "Stability theory for a pair of trailing vortices," AIAA J. **8**, 2172 (1970).

[15]F. W. Dyson, "The potential of an anchor ring. Part II," Philos. Trans. R. Soc. London, Ser. A **184**, 1041 (1893).

[16]Y. Fukumoto, "Higher-order asymptotic theory for the velocity field induced by an inviscid vortex ring," Fluid Dyn. Res. **30**, 65 (2002).

[17]C. Tung and L. Ting, "Motion and decay of a vortex ring," Phys. Fluids **10**, 901 (1967).

[18]P. G. Saffman, "The velocity of viscous vortex rings," Stud. Appl. Math. **49**, 371 (1970).

[19]Y. Fukumoto and H. K. Moffatt, "Motion and expansion of a viscous vortex ring. Part 1. A higher-order asymptotic formula for the velocity," J. Fluid Mech. **417**, 1 (2000).

[20]T. Levi-Civita, "Attrazione Newtoniana dei tubi sottili e vortici filiformi (Newtonian attraction of slender tubes and filiform vortices," Annali della Scuola Normale Superiore di Pisa **1**, 229 (1932).

[21]R. L. Ricca, "The contributions of Da Rios and Levi-Civita to asymptotic potential theory and vortex filament dynamics," Fluid Dyn. Res. **18**, 245 (1996).

[22]V. L. Okulov, "On the stability of multiple helical vortices," J. Fluid Mech. **521**, 319 (2004).

[23]Y. Fukumoto, "Three-dimensional motion of a vortex filament and its relation to the localized induction hierarchy," Eur. Phys. J. B **29**, 167 (2002).

[24]J. Segata, "Well-posedness for the fourth order nonlinear Schrödinger type equation related to the vortex filament," Diff. Integral Eq. **16**, 841 (2003).

[25]A. J. Callegari and L. Ting, "Motion of a curved vortex filament with decaying vortical core and axial velocity," SIAM J. Appl. Math. **35**, 148 (1978).

[26]Y. Fukumoto and T. Miyazaki, "Three-dimensional distortions of a vortex filament with axial velocity," J. Fluid Mech. **222**, 369 (1991).

[27]G. N. Watson, *A Treatise on the Theory of Bessel Functions* (Cambridge University Press, Cambridge, 1922).

[28]D. H. Wood and J. Boersma, "On the motion of multiple helical vortices," J. Fluid Mech. **447**, 149 (2001).

[29]S. Leibovich, "Vortex stability and breakdown: Survey and extension," AIAA J. **22**, 1192 (1984).

[30]M. P. Escudier, "Vortex breakdown: observations and explanations," Prog. Aerosp. Sci. **25**, 189 (1988).

[31]M. R. Ruith, P. Chen, E. Meiburg, and T. Maxworthy, "Three-dimensional vortex breakdown in swirling jets and wakes: Direct numerical simulation," J. Fluid Mech. **486**, 331 (2003).

[32]L. E. Fraenkel, "Examples of steady vortex rings of small cross-section in an ideal fluid," J. Fluid Mech. **51**, 119 (1972).

[33]Y. Hattori and Y. Fukumoto, "Short-wavelength stability analysis of thin vortex rings," Phys. Fluids **15**, 3151 (2003).

[34]Y. Fukumoto and Y. Hattori, "Curvature instability of a vortex ring," J. Fluid Mech. **526**, 77 (2005).

[35]R. Klein and A. J. Majda, "Self-stretching of a perturbed vortex filament. I. The asymptotic equation for deviations from a straight line," Physica D **49**, 323 (1991).

[36]T. S. Lundgren and W. T. Ashurst, "Area-varying waves on curved vortex tubes with application to vortex breakdown," J. Fluid Mech. **200**, 283 (1989).

[37]A. Leonard, "Nonlocal theory of area-varying waves on axisymmetric vortex tubes," Phys. Fluids **6**, 765 (1994).

[38]S. E. Widnall, D. B. Bliss, and A. Zalay, "Theoretical and experimental study of the stability of a vortex pair," in *Aircraft Wake Turbulence and its Detection*, edited by J. H. Olsen, A. Goldburg, and M. Rogers (Plenum, New York, 1971), pp. 305–338.

[39]M. Abramowitz and I. A. Stegun, *Handbook of Mathematical Functions* (Dover, New York, 1965).